Chapter 6
Engine Performance Analysis

Abbreviations and Symbols

ADC	Analog-to-digital converter
BDC	Bottom dead center
BMEP	Brake mean effective pressure
BSFC	Brake-specific fuel consumption
CCVL	Continuous variable valve lift
CDC	Conventional diesel combustion
CR	Compression ratio
CW	Counter weight
DPI	Difference pressure integral
EGR	Exhaust gas recirculation
F/*A*	Fuel-air ratio
GDI	Gasoline direct injection
HCCI	Homogeneous charge compression ignition
IMEP	Indicated mean effective pressure
MEP	Mean effective pressure
NMEP	Net mean effective pressure
PFI	Port fuel injection
PMEP	Pumping mean effective pressure
RCCI	Reactivity controlled compression ignition
SI	Spark ignition
SOE	Start of energizing
TDC	Top dead center
VVL	Variable valve lift
VVT	Variable valve timing
D	Diameter of the cylinder
P	Cylinder pressure
R	Crankshaft radius

R. K. Maurya, *Reciprocating Engine Combustion Diagnostics*, Mechanical Engineering Series, https://doi.org/10.1007/978-3-030-11954-6_6

V	Volume of cylinder
X	Number of revolution per engine cycle
a	Acceleration of piston
A_{p}	Piston area
F_{e}	Engine flexibility
F_{IP}	Inertial force on piston
F_{N}	Engine speed flexibility
F_{P}	Piston force
F_{T}	Thrust force
I_{S}	Moment of inertia of crankshaft
m_{f}	Mass of fuel burned per cycle
m_{p}	Mass of piston
N_{P}	Engine speed at maximum power
N_{T}	Engine speed at maximum torque
P_{b}	Brake work
P_{i}	Indicated power
P_{in}	Intake pressure
Q_{LHV}	Lower heating value of the fuel
R_{bs}	Ratio of cylinder bore to stroke
r_{c}	Compression ratio
T_{e}	Engine torque
T_{IS}	Inertial torque on the crankshaft
T_{max}	Maximum engine torque
V_{c}	Clearance volume
V_{d}	Displacement volume
V_{p}	Piston velocity
W_{b}	Brake work
W	Indicated work
W_{pump}	Pumping work
α_{c}	Angular acceleration of connecting rod
α_{e}	Angular acceleration of engine
η_{b}	Brake efficiency
η_{c}	Combustion efficiency
$\eta_{\mathrm{g,i}}$	Gross indicated efficiency
η_{ge}	Gas exchange efficiency
η_{m}	Mechanical efficiency
$\eta_{\mathrm{n,t}}$	Net indicated efficiency
η_{tm}	Thermodynamic efficiency
ω_{c}	Angular velocity of connecting rod
ω_{e}	Angular velocity of engine
θ	Crankshaft position
ϕ	Equivalence ratio

6.1 Indicating Diagram Analysis

Engine performance generally means how well an engine is producing power (output) with respect to energy input or how effectively it provides useful energy with respect to some other comparable engine. Several measurable parameters are developed to determine and compare the engine performance for a particular engine as well as engines of different sizes. To maximize the performance of a particular engine, the developer must understand the combustion process and identify the inadequately designed components. Cylinder pressure-based combustion diagnostics can be used to understand the engine combustion process and to set the optimal engine operating conditions. It can also provide the direction to design or modify a particular engine component for better engine performance.

Accurate cylinder pressure can be acquired by instrumenting the engine (Chap. 2) and appropriately processing the recorded signal (Chap. 5). The measured pressure data can be graphically presented in typically three ways as shown in Fig. 6.1. The measured in-cylinder pressure data can be presented as a function of crankshaft position (P-θ) or combustion chamber volume with linear (P-V) as well as log scale ($\log P - \log V$), and each representation has its own particular characteristics

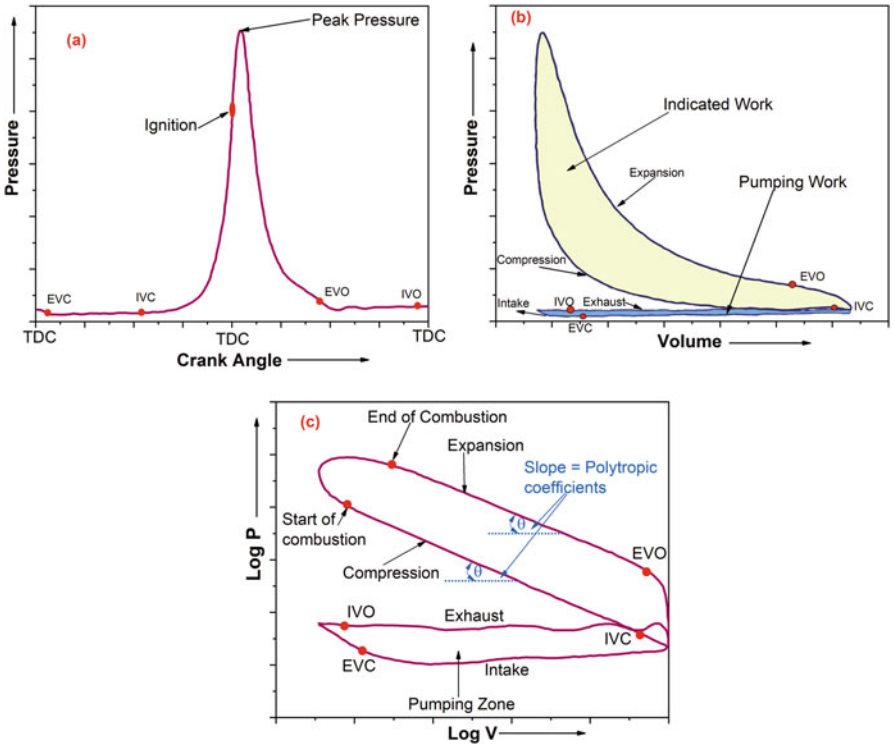

Fig. 6.1 Graphical representation of measured cylinder pressure data of one engine cycle

[1]. Crank angle-based events such as valve openings and closings, ignition and injection timings, etc. can be clearly identified in the P-θ diagram (Fig. 6.1a). In the P-V diagram (Fig. 6.1b), areas of loops represent the work produced by the engine. Area of the upper loop consisting compression and expansion strokes shows the indicated work produced in the cycle, and area of the lower loop consisting intake and exhaust strokes shows the pumping work required in the engine cycle (Fig. 6.1b). In case of the $\log P - \log V$ diagram (Fig. 6.1c), the compression and expansion strokes are linear (straight line) before the start of combustion and after the end of combustion due to polytropic (adiabatic) relation between pressure and volume curve. The slopes of the straight lines in compression and expansion stroke are equal to the polytropic compression and expansion coefficients, respectively (Fig. 6.1c). Additionally, in this curve, the pumping loop is considerably expanded.

The cylinder pressure measurements and its adequate analysis can provide information regarding cylinder balance, combustion phasing, knocking, intake and exhaust tuning, cyclic torque variability, structural loading, thermal efficiency, and cyclic fueling variability. Effective analysis of these combustion and performance parameters often depends on the accuracy of the measured cylinder pressure data. Typical sources of error in the cylinder pressure measurement include absolute pressure offset, inaccurate measurement system calibration, incorrect crank angle phasing, sensitivity changes due to temperature variations, long-term drift, thermal shock distortion/short-term drift, effects due to transducer mounting, coarse analog-to-digital conversion and crank angle resolutions, mechanical vibration noise, and electrical noise [2]. The significance of each of these sources of errors in the cylinder pressure measurement is dependent on the analysis being performed using the measured pressure data.

Figure 6.2 illustrates the how different types of measurement error manifests in the cylinder pressure signal. The errors due to incorrect pegging (referencing) with cylinder volume leads to shift in the cylinder pressure signal (Fig. 6.2) as these errors typically change/shift the absolute value of pressure at the particular crank position. Thus, work calculation is not affected by this error because the area of the loop remains the same. Valve-closing noise occurs at the time of valve closure and appears in the cylinder pressure data as shown in Fig. 6.2. Valve-closing noise is a result of (1) overly accelerating the transducer (high-amplitude vibration) which generates an acoustic wave at valve impact and (2) from the fast changing stress distribution in the engine structure (specifically in the transducer mount) [1]. The amplitude of the valve noise rapidly declines after the first period (highest amplitude). Typically, valve closure noise is not an issue in production engines because the valve-seating velocities are considerably lower. Thermal shock is one of the major errors in the cylinder pressure measurement. The thermal shock causes the measured pressure early in the exhaust stroke to be considerably below the actual value (Fig. 6.2). Measurement error due to thermal shock is highest when the flame from the combustion process reaches the pressure transducer. Thermal shock gradually decreases after this point until the next combustion event. Several solutions are proposed to thermal shock problem such as water cooling, heat shield, appropriate sensor mounting position, etc. (Chap. 2). Electrical noise can appear on the cylinder

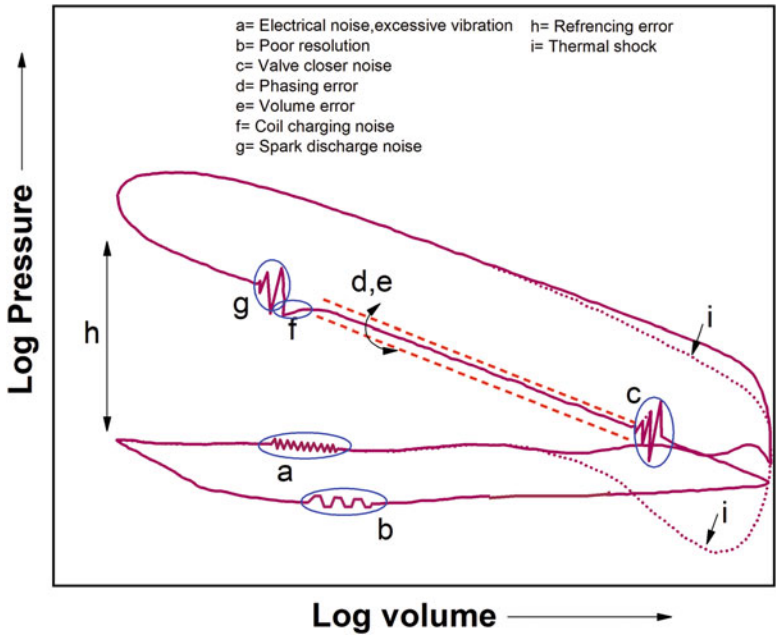

Fig. 6.2 Illustration of different types of cylinder pressure measurement error (adapted from [1])

pressure data in many different forms. One common source is conducted noise produced by the formation of a ground potential during coil charging. Another form of noise, namely, radiated noise which occurs at the time of spark discharge, may become prevalent in race engine applications. The electrical noise from each source has a distinct appearance [1]. To avoid some of the electrical noise, all instrumentation attached to the engine must be properly grounded and preferably shielded. Pressure signal needs to be recorded at sufficient resolution, and poor resolution leads to an error in representing the pressure signal (Fig. 6.2). However, a very high-resolution recording of cylinder pressure data leads to a large amount of data that can create data handling issues during post-processing.

Cylinder pressure signal measured with sufficient accuracy can be used for further processing and analysis. Presentation of the measured pressure signal with crank angle position or cylinder volume also provides various information regarding the performance, combustion, different losses, and design of components. Figure 6.3 illustrates the variations between thermodynamic air cycle and the actual cycle in a P-V and log P − log V diagram. The various losses can be identified by comparing the measured cylinder pressure and the cylinder pressure of an idealized cycle (Fig. 6.3). The addition of heat is typically assumed to be instantaneous, but in the actual engine cycle, the combustion of air-fuel mixture takes a finite amount of time. The non-instantaneous burning causes a reduction in the net area of the P-V diagram, which indicates a loss in work. This phenomenon is typically termed as time loss [3]. Typically, in the ideal cycle, adiabatic processes (no heat loss) are considered

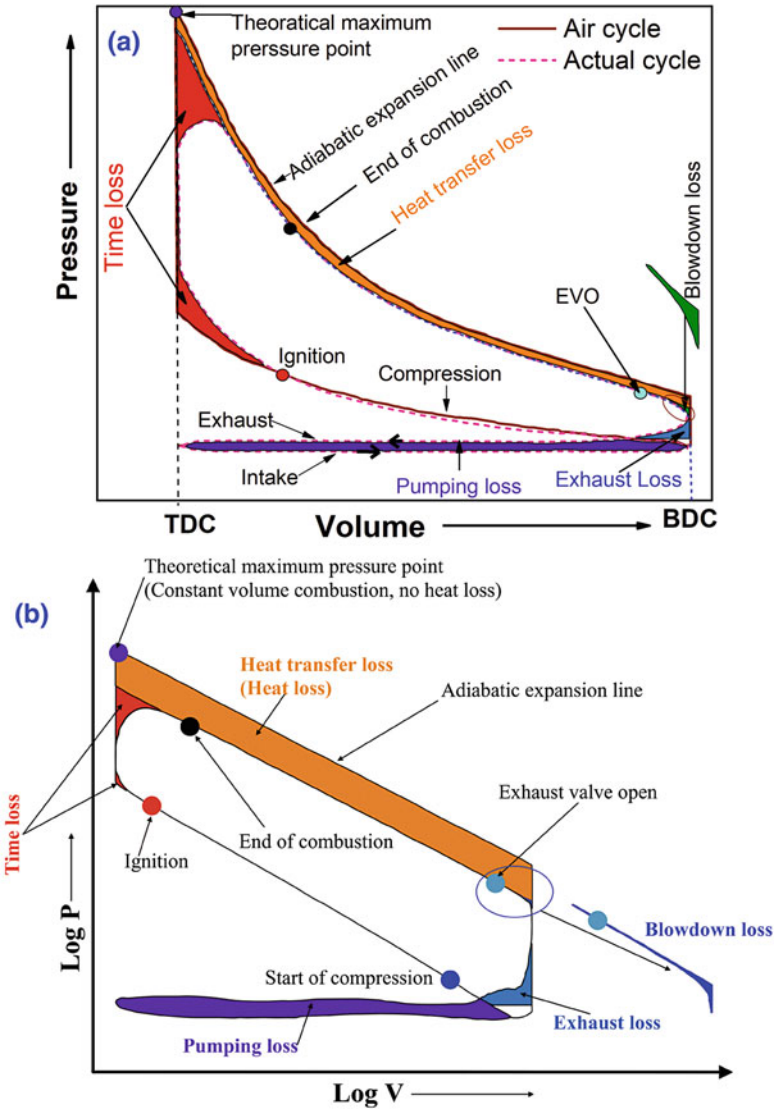

Fig. 6.3 Comparison of thermodynamic air cycle and actual cycle indicating various losses in the actual engine cycle (adapted from [3, 4])

during compression and expansion. However, the actual cycle has heat losses in the combustion chamber area, which reduces the work produced by the engine. In the ideal cycle, the instantaneous heat rejection is assumed, which is not possible in the actual cycle due to the inertia of the exhaust valve and exhaust gases. Thus, the exhaust valve opens before the piston reaches BDC position, leading to the blow-down losses. All the combustion products are not exhausted during exhaust stroke

due to clearance volume. The residual gases mix with fresh charge inducted in the cycle leading to dilution and heating it, which lowers the work produced in the cycle, and termed as exhaust loss. The pressure in the cylinder is different during intake and exhaust stroke, which leads to the pumping losses. Pumping work (lower loop) is considered as loss because piston has to do the work on the gases in the cylinder. Typically, at part-load condition in SI engine, the area of the lower loop (pumping loss) increases due to restriction in air flow by the throttle.

Comparing measured in-cylinder pressure curve at different engine operating conditions also provide useful information to optimize several parameters such as the ignition timing, injection timings, valve timings, etc. for maximum thermal efficiency and lower exhaust emissions. The shape of indicator diagram provides an indication of how various processes are affecting the combustion and work produced in the cycle. Figure 6.4 shows the effect of advanced and retarded (late)

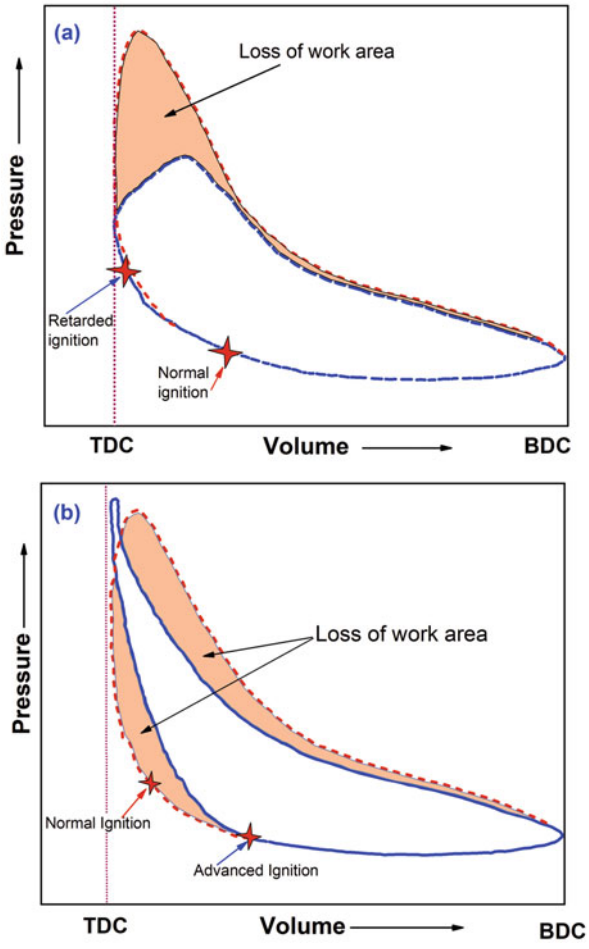

Fig. 6.4 Effect of (**a**) retarded spark timings and (**b**) advanced spark timing on work produced in the cycle (adapted from [3])

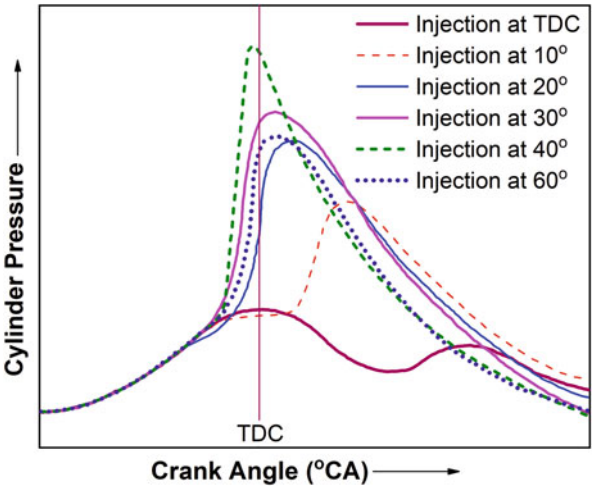

Fig. 6.5 Effect of fuel injection timing on cylinder pressure in a diesel engine (adapted from [3])

ignition timing on the work produced in the cycle. The figure clearly depicts the work loss (reduced loop area) in both advanced and retarded ignition timings. In case of retarded ignition timings, the peak pressure occurs when the piston is significantly away from TDC position due to finite time required for burning fuel-air mixture in the combustion chamber. Thus, the indicated work area is reduced, and lower work is obtained in this condition (Fig. 6.4a). When the spark timing is advanced, the combustion starts early, and pressure in the cylinder starts rising, which works against the piston motion. Thus, the indicated work area will be smaller than normal spark timings (Fig.6.4b) leading to lower work production in the cycle.

Similarly, cylinder pressure versus crank position (P-θ) can also be used for combustion analysis. The evolution of pressure as a function of crankshaft position and pressure rise rate is well presented in this curve. Figure 6.5 shows the *P-θ* diagram illustrating the effect of fuel injection timing in a compression ignition engine. The figure shows the how peak pressure and pressure rise rate are affected by fuel injection timings. For very late injection timings, the peak pressure is significantly lower because pressure rise due to combustion is utilized by overcoming the expansion of cylinder volume. Fuel injection 40° before TDC produces considerably higher peak pressure as well as higher pressure rise rate. For the injection timing much earlier (60° before TDC), the peak pressure again decreases (Fig. 6.5) due to sluggish burning [3]. For too early injection timing, the fuel is not properly prepared for rapid combustion due to lower air temperature at the timing of fuel injection. Thus, fuel injection timing can be adjusted to produce maximum power without engine roughness or emissions with the help of cylinder pressure measurement and its analysis.

The indicating diagram can be used to analyze the intake or exhaust manifold design as well the valve timings with respect to pumping loss evaluation. Figure 6.6 illustrates the effect of the improper design of intake/exhaust and improper valve timings on *P-V* diagram. If restrictions are imposed on the flow of charge through

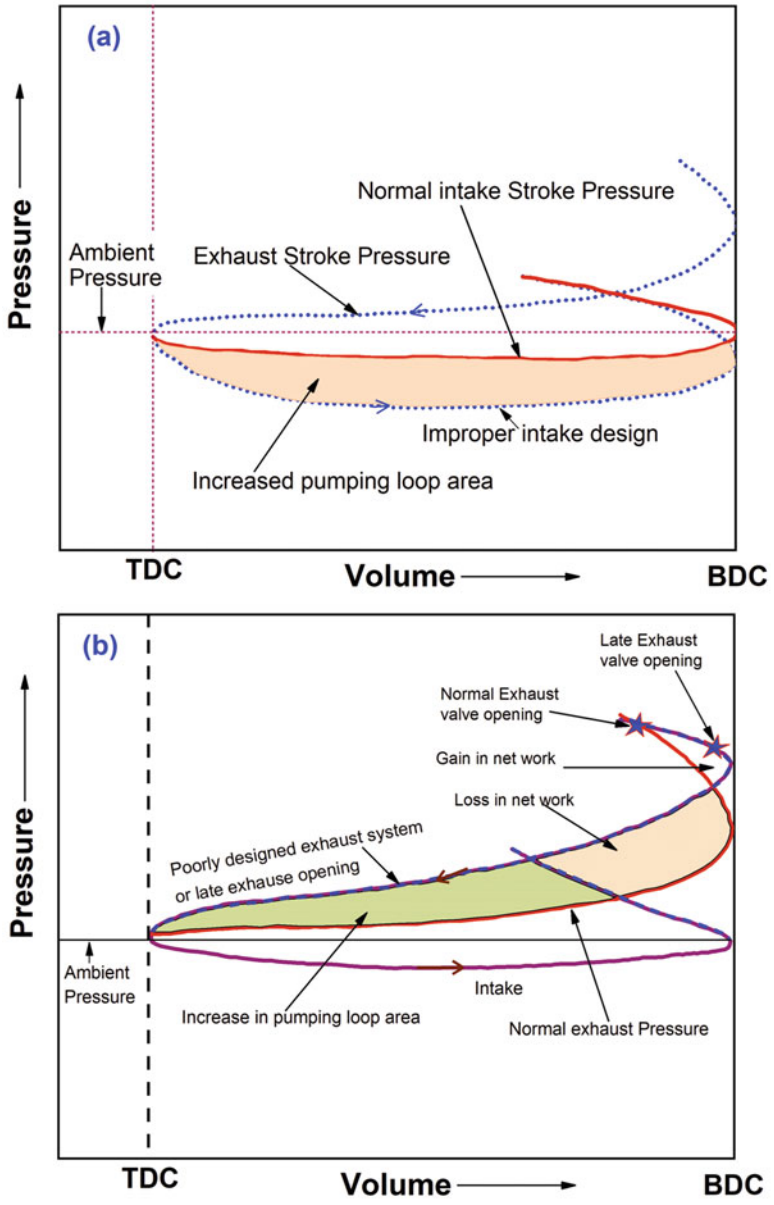

Fig. 6.6 Effect of (**a**) improper intake design and (**b**) exhaust valve opening on the pressure curve (adapted from [3])

intake system by undersized valves or other impediments, the reduction in pressure occurs, which reflect as pumping work requirement by increasing the area of pumping loop (Fig. 6.6a). Similarly, improper exhaust design or late valve opening

timings leads to higher pressure in the exhaust stroke which leads to increasing the area of pumping loop. Thus, pumping work is increased due to improper design or valve timings, which can be optimized based on cylinder pressure measurement.

The measured cylinder pressure can be further processed to calculate other combustion and performance parameters. Combustion parameters and heat release calculation based on measured cylinder pressure are discussed in Chap. 7. Performance parameters such as indicated work, indicated torque, engine efficiency, etc. are discussed in the next section of the present chapter.

6.2 Engine Geometry and Kinematics

The kinematics of a reciprocating engine is similar to a slider-crank mechanism. Figure 6.7 shows a simplified reciprocating mechanism of the engine along with different terminologies used for characterizing engine geometry. The topmost piston position is defined as the top dead center (TDC), and the bottom most position is termed as a bottom dead center (BDC). The movement of the piston with respect to TDC position is denoted by variable $x(\theta)$, and the total distance traveled between

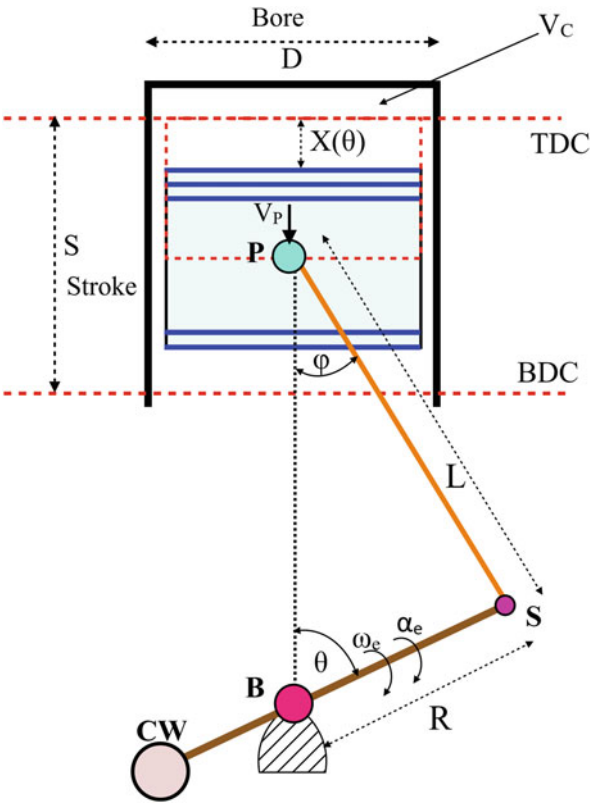

Fig. 6.7 Engine geometry and terminology

TDC and BDC position is defined as stroke (S). The diameter (D) of the cylinder is known as engine bore. The crankshaft radius is denoted as R, and connecting rod length is L. The connecting rod is joined to the piston via gudgeon pin or wrist pin (Point P) and to the crankshaft at point S using journal bearing. Crankshaft is supported on the main engine bearing (Point B). Typically, a counterweight (CW) is used for balancing the engine crankshaft.

The basic geometry of a reciprocating engine is defined by compression ratio, the ratio of cylinder bore to piston stroke (R_{bs}), and the ratio of crankshaft radius to connecting rod length (λ).

The compression ratio (r_c) is shown in Eq. (6.1).

$$\text{Compression ratio } (r_c) = \frac{\text{Volume at BDC position}}{\text{Volume at TDC position}} = \frac{V_d + V_c}{V_c} \tag{6.1}$$

where V_c is the clearance volume and V_d is swept or displacement volume. The relation between total volume (V), clearance volume, and swept volume are shown in Eqs. (6.2)–(6.4).

$$V(\theta) = V_c + x(\theta)\frac{\pi D^2}{4} \tag{6.2}$$

$$V_c = \frac{\pi D^2 R}{2(r_c - 1)} \tag{6.3}$$

$$V_d = \frac{\pi D^2 S}{4} \tag{6.4}$$

The ratio of the cylinder bore to piston stroke (D/S) is typically 0.8–1.2 for small- and medium-size engines and about 0.5 for large slow speed engines [5]. The ratio of crank radius (R) to connecting rod length (L) is denoted as λ ($=R/L$) typically less than one for all practical purpose, and its value ranges from 0.33 to 0.25 for small- to medium-size engine and 0.2 to 0.11 for larger slow speed engines.

The displacement of the piston as a function of crankshaft position (θ) can be calculated from engine geometry by Eq. (6.5).

$$x(\theta) = (L + R) - (R\cos\theta + L\cos\phi) \tag{6.5}$$

The sine law of trigonometry defines the relationship between θ and ϕ by Eq. (6.6).

$$L\sin\phi = R\sin\theta \tag{6.6}$$

Thus,

$$\sin\phi = \frac{R}{L}\sin\theta = \lambda\sin\theta \tag{6.7}$$

$$\cos\phi = \sqrt{1 - \lambda^2 \sin^2\theta} \tag{6.8}$$

The $x(\theta)$ can be written in terms of engine geometry as Eq. (6.9).

$$x(\theta) = (L + R) - \left(R\cos\theta + L\sqrt{1 - \lambda^2 \sin^2\theta}\right) \tag{6.9}$$

Differentiation of Eq. (6.9) provides the piston velocity (V_p).

$$\frac{dx}{d\theta} = R(-\sin\theta) + \frac{L}{2} \times \frac{-\lambda^2 2\sin\theta\cos\theta}{\sqrt{1 - \lambda^2 \sin^2\theta}} = -R\left[(\sin\theta) + \frac{\lambda}{2}\frac{\sin 2\theta}{\sqrt{1 - \lambda^2 \sin^2\theta}}\right] \tag{6.10}$$

Piston velocity in terms of engine speed (ω_e) can be calculated as shown in Eqs. (6.11) and (6.12).

$$\frac{dx}{d\theta} = \frac{dx}{dt} \cdot \frac{dt}{d\theta} = \frac{dx}{dt}\frac{1}{\omega} = \frac{V_p}{\omega} \tag{6.11}$$

$$V_p = -\omega_e R\left[\sin\theta + \frac{\lambda}{2}\frac{\sin 2\theta}{\sqrt{1 - \lambda^2 \sin^2\theta}}\right] = -\omega_e R\left[\sin\theta + \frac{\lambda}{2}\frac{\sin 2\theta}{\cos\phi}\right] \tag{6.12}$$

The acceleration of piston (a_p) can be obtained by differentiating the piston velocity (V_p), and the result is shown in Eq. (6.13) at constant engine speed (ω_e).

$$\begin{aligned}\frac{V_p}{dt} = a_p &= -{\omega_e}^2 R\left[\cos\theta + \frac{\lambda\cos 2\theta}{\sqrt{1 - \lambda^2 \sin^2\theta}} + \lambda^3 \frac{\sin^2\theta\cos^2\theta}{\left(\sqrt{1 - \lambda^2 \sin^2\theta}\right)^3}\right] \\ &= -{\omega_e}^2 R\left[\cos\theta + \frac{\lambda\cos 2\theta}{\cos\phi} + \lambda^3 \frac{\sin^2\theta\cos^2\theta}{(\cos\phi)^3}\right]\end{aligned} \tag{6.13}$$

When the engine is accelerating with angular acceleration (α_e), then piston acceleration (a_p) can be represented by Eq. (6.14).

$$a_p = -{\omega_e}^2 R\left[\cos\theta + \frac{\lambda\cos 2\theta}{\cos\phi} + \lambda^3 \frac{\sin^2\theta\cos^2\theta}{(\cos\phi)^3}\right] - \alpha_e R\left[\sin\theta + \frac{\lambda}{2}\frac{\sin 2\theta}{\cos\phi}\right] \tag{6.14}$$

However, the additional second term (due to angular acceleration of engine) in Eq. (6.14) is typically very small and negligible in comparison to the first term, particularly at top engine speeds. Therefore, it is reasonable to always use Eq. (6.13) for calculation of piston acceleration even in accelerating condition of the reciprocating engine [6].

The equation of piston speed and acceleration are highly nonlinear in nature, and they can be simplified by using Taylor series expansion as $\lambda^2 \sin^2\theta \ll 1$. The Eqs. (6.12) and (6.13) can be written as Eqs. (6.15) and (6.16) [7].

$$V_p = -\omega_e R\left[\sin\theta + \frac{A_2}{2}\sin 2\theta - \frac{A_4}{4}\sin 4\theta + \cdots\right] \tag{6.15}$$

$$a_p = -{\omega_e}^2 R[\cos\theta + A_2\cos 2\theta - A_4\cos 4\theta + \cdots] \tag{6.16}$$

where

$$A_2 = \lambda + \frac{\lambda^3}{4} + \frac{15\lambda^5}{128} + \cdots \tag{6.17}$$

$$A_4 = \frac{\lambda^3}{4} + \frac{3\lambda^5}{16} + \cdots \tag{6.18}$$

when $\lambda \ll 1$, neglecting the λ^3 or higher powers of λ, the piston velocity and acceleration can be easily calculated by Eqs. (6.19) and (6.20).

$$V_p = -\omega_e R\left(\sin\theta + \frac{\lambda}{2}\sin 2\theta\right) \tag{6.19}$$

$$a_p = -{\omega_e}^2 R(\cos\theta + \lambda\cos 2\theta) \tag{6.20}$$

After calculating the kinematics of piston, the kinematics of the connecting rod including the rotation speed and acceleration of its center of gravity position (Point G) can be estimated using classical dynamics. Figure 6.8 shows the kinematics terminology of the connecting rod.

The velocity and acceleration vectors of point S (where the shaft is joined with connecting rod) can be written in terms of angular velocity and acceleration of engine crankshaft. The velocity and acceleration of point S on the crankshaft can be written as Eqs. (6.21) and (6.22). Radius vector $\vec{R}$ is from the main bearing (point B) to point S. Perpendicular unit vectors are shown in Fig. 6.8.

$$\vec{V}_s = \vec{\omega}_e \times \vec{R} \tag{6.21}$$

$$\vec{\alpha}_S = \vec{\alpha}_e \times \vec{R} + \vec{\omega}_e \times \left(\vec{\omega}_e \times \vec{R}\right) \tag{6.22}$$

$$\vec{\omega}_e = -\omega_e \hat{k} \tag{6.23}$$

$$\vec{\alpha}_e = -\alpha_e \hat{k} \tag{6.24}$$

$$\vec{R} = R\sin\theta\hat{i} + R\cos\theta\hat{j} \tag{6.25}$$

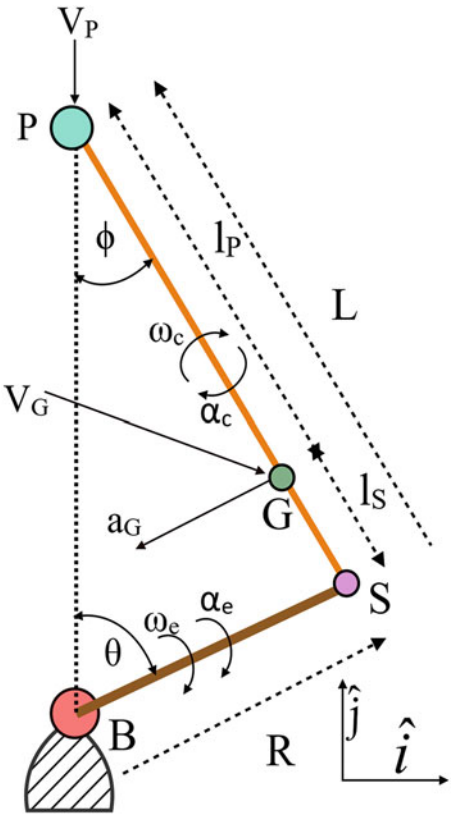

Fig. 6.8 Kinematics terminology of connecting road and crankshaft

The solution of Eqs. (6.21) and (6.22) provides the velocity and acceleration of point S.

$$\vec{V}_S = R\omega_e\left(\cos\theta\hat{i} - \sin\theta\hat{j}\right) \tag{6.26}$$

$$\vec{\alpha}_S = R\left(\alpha_e\cos\theta - \omega^2{}_e\sin\theta\right)\hat{i} - R\left(\alpha_e\sin\theta + \omega^2{}_e\cos\theta\right)\hat{j} \tag{6.27}$$

The angular velocity (ω_c) and angular acceleration of the connecting rod can be easily calculated by knowing the velocity and acceleration of two points (S and P) on the connecting rod (rigid body). The angular velocity (ω_c) and acceleration (α_c) of connecting rod are related with two points by Eqs. (6.28) and (6.29) [6].

$$\vec{V}_S = \vec{V}_P + \vec{\omega}_c \times \vec{L} \tag{6.28}$$

$$\vec{a}_S = \vec{a}_P + \vec{\alpha}_C \times \vec{L} + \omega_c\left(\vec{\omega}_c \times \vec{L}\right) \tag{6.29}$$

where:

$$\vec{\omega}_c = -\omega_c \hat{k} \tag{6.30}$$

$$\vec{\alpha}_c = -\alpha_c \hat{k} \tag{6.31}$$

A solution of Eqs. (6.28) and (6.29) provides the angular velocity and acceleration of the connecting rod of the engine [6].

$$\omega_C = -\frac{R}{L} \cdot \frac{\cos\theta}{\cos\phi} \omega_e \tag{6.32}$$

$$\alpha_C = -\frac{R}{L} \cdot \frac{\cos\theta}{\cos\phi} \alpha_e + \frac{R}{L} \cdot \frac{\sin\theta}{\cos\phi} \omega_e^2 \tag{6.33}$$

The velocity and acceleration of the center of gravity of connecting rod (point G) can be estimated by considering the angular velocity and acceleration of rod and velocity and acceleration of any other point on the rod (point P or point S) using the equations similar to Eqs. (6.28) and (6.29). The velocity and acceleration of point G can be written as Eqs. (6.34) and (6.35).

$$\vec{V}_G = R\omega_e \left(C_1 \hat{i} + C_2 \hat{j}\right) \tag{6.34}$$

$$\vec{a}_G = R\alpha_e \left(C_1 \hat{i} + C_2 \hat{j}\right) - R\omega_e^2 \left(C_3 \hat{i} + C_4 \hat{j}\right) \tag{6.35}$$

where:

$$C_1 = \frac{l_A}{L} \cos\theta \tag{6.36}$$

$$C_2 = -\left(1 + \lambda \cdot \frac{\cos\theta}{\cos\phi} \cdot \frac{l_B}{L}\right) \sin\theta \tag{6.37}$$

$$C_3 = \frac{l_A}{L} \sin\theta \tag{6.38}$$

$$C_4 = \cos\theta + \lambda \cdot \frac{\cos 2\theta}{\cos\phi} \cdot \frac{l_B}{L} \tag{6.39}$$

Kinematic parameters of the connecting rod can be used in the determination of engine torque. Most important kinematic parameters are piston speed and piston acceleration. Typical variations of piston speed and acceleration as a function of crankshaft position at different engine speed are shown in Fig. 6.9. The peak piston speed and acceleration increase with engine speed. Piston speed attains zero value at both TDC and BDC positions, and reaches its peak value in the between TDC and BDC position. The variation in piston speed leads to differences in time travel in

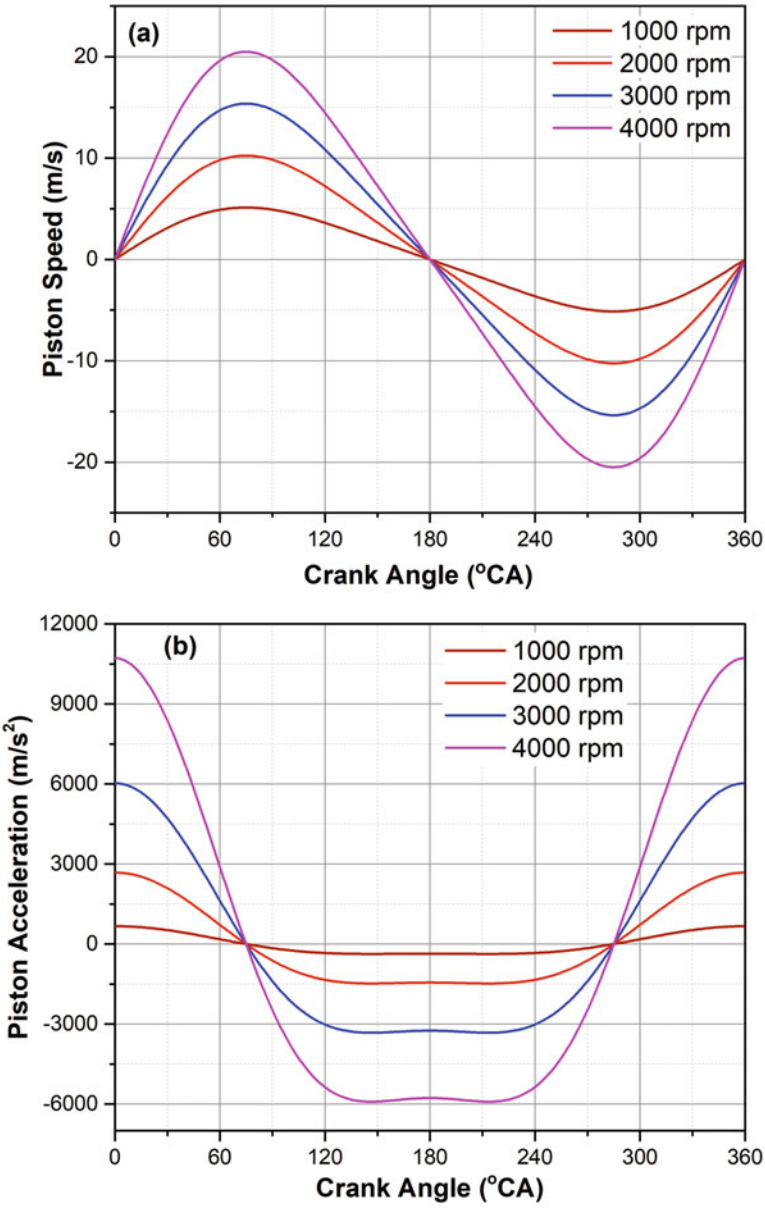

Fig. 6.9 Variations of piston speed and acceleration with crank angle position at different engine speeds of a typical engine

terms of crank angle depending on the position of the piston. Figure 6.9 also shows that the peak piston speed is not at exactly in the middle of the stroke, which can also be confirmed by the position where acceleration is zero. The peak position of piston speed depends on the rod ratio (λ) of the engine.

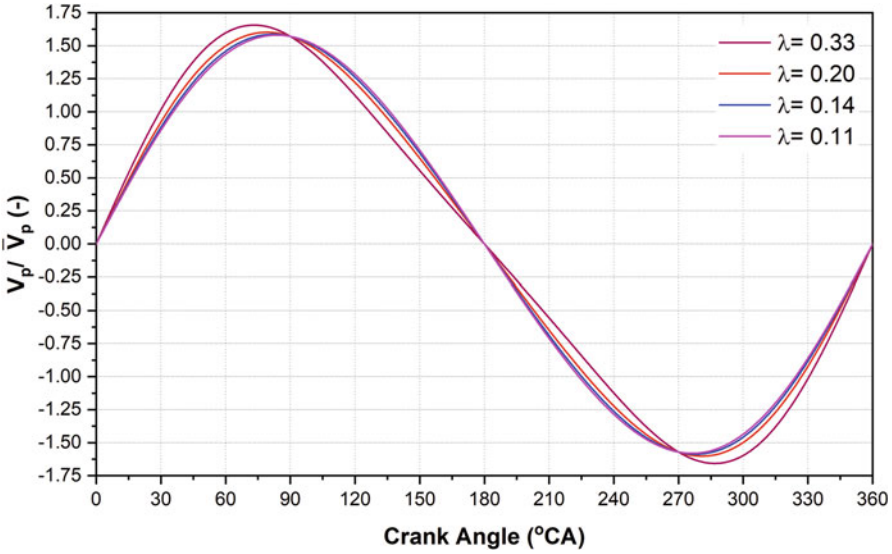

Fig. 6.10 Variations of piston speed as a function of crank angle at different rod ratios for a typical engine

Figure 6.10 shows the variation of piston speed as a function of crank angle at different rod ratios. Piston speed is normalized by dividing with mean piston speed. For relatively shorter connecting rod, the peak piston speed occurs early before the middle position of stroke (Fig. 6.10). It can be observed from Fig. 6.10 that relatively shorter connecting rod is slower at BDC range and faster at TDC range, and longer connecting rod is faster at BDC range and slower at TDC range.

In case of longer connecting rod, the piston moves slower during the middle of stroke to TDC position which may lead to a change in ignition timing because more time is spent due to lower piston speed. In expansion stroke, longer connecting rod spends less time for the travel from the middle of stroke to BDC, which makes less time availability for the exhaust to escape at the time of exhaust valve opening. The longer connecting rod engines could have relatively higher pumping losses. Shorter connecting rod spends less time near TDC position. Thus, it will suck air harder in the early part of the intake stroke and exerts more force to the crank pin before the middle of the power stroke. Thus, shorter connecting rod engines may require stronger wrist pins, piston pin bosses, and connecting rods than a relatively longer connecting rod. Shorter connecting rod spends more time at the bottom which can be beneficial in reducing intake charge being pumped back out in the intake manifold as the valve closes. Thus, varying the connecting rod ratio (λ) changes the instantaneous piston speed near TDC for a particular engine.

The mean piston speed is a measure for comparing the drives of various engines. Mean piston speed provides information on the engine load on the sliding partners and indications of the power density of the engine [8]. Typically, mean piston speed

is between 8 and 15 m/s for typical automotive engines, and it is higher for racing engine up to 33 m/s [5, 9]. The mean piston speed can be calculated using Eq. (6.40).

$$\overline{V}_{\mathrm{p}} = \frac{1}{\pi}\int_{180}^{360} V_{\mathrm{p}}(\theta)d\theta = 2SN \tag{6.40}$$

where S is the stroke length and N is the engine speed.

The mean piston speed increases with an increase in the rotational engine speed. The mean piston speed is comparable among different types of reciprocating engines, and it is a better metric than engine speed (rpm). The mean piston velocity also defines the engine design limits. The mean piston speed affects the frictional losses and the gas exchange process significantly. Gas flow velocities in the intake manifold and gas flow velocities in the combustion chamber scales with mean piston speed. Thus, gas flow through valves and turbulent velocity of flow in the cylinder are related with mean piston speed. Typically, maximum gas flow is limited by the occurrence of sonic flow (Mach number equal to one) in the valve aperture [10]. Frictional power loss is related to engine speed via second-order polynomial. Thus, mechanical efficiency will be dependent on mean piston speed independent of engine size. The mechanical efficiency at lower speed is around 0.85 at low engine speed and drops to 0.6 at a mean piston speed of 20 m/s. This is almost independent of engine size because piston rings and cylinder are made of roughly same material, and lubricating oils are also used of similar viscosity [10]. Temperature rise of engine components such as exhaust valves and piston crowns is typically proportional to the turbulent velocity that is roughly proportional to the piston speed. A high mean piston speed is one of the structural limits imposed on any engine design [9]. The inertial forces, frictional wear, gas flow resistance during intake, and engine noise also increase at higher mean piston speed. Typically, inertial forces on connecting rods (and other reciprocating components) are proportional to the square of the piston speed (see Eqs. 6.20, 6.27, 6.33, and 6.35). Maximum allowed inertial forces limit the mean piston speed and, thus, engine speed. The engine speed is also limited by another constraint of time required for fuel-air mixture formation in the combustion chamber for reciprocating engines with internal charge preparation (direct fuel injection) such as diesel engine.

6.3 Indicated Torque Calculation and Analysis

To characterize the operating status and performance of an engine, torque is one of the key parameters. The engine torque is directly related with the drivability and the responsiveness of the automotive vehicle. The driver of the vehicle can feel the torque produced by the engine, and it is also a contributing factor in customer satisfaction. Thus, the sophisticated control of torque is required on an automotive engine [11]. Cylinder pressure measurement provides new opportunities for

advanced closed-loop control, which leads to a reduction in engine emissions and improved fuel conversion efficiency [12].

Indicated torque (gas torque) is one of the parameters that can be calculated from the measured cylinder pressure data. The indicated torque is the main contributor to the output torque from the engine crankshaft. The other contributing factors are friction torque and mass torque imposed by the piston assembly. Various ways of engine torque estimation are explored because direct measurement of shaft torque using torque sensor encounters problems in cost, reliability, and vibration/noise immunity [11]. Engine torque estimation using instantaneous crank angle fluctuation is proposed by several studies [13–16]. This method of torque estimation employs a dynamic model of the engine shaft and the frequency spectrum of the measured engine speed. This method is simple and easy to implement, but it has inaccuracy [15, 17]. Engine torque can also be calculated from indicated mean effective pressure (IMEP) which is estimated from measured cylinder pressure data [5, 11].

The estimation of the indicated torque is possible using cylinder pressure measurement, which eliminates the requirement of an indicated torque model. The combustion process in the cylinder leads to high cylinder pressure that exerts a force on the top surface of the piston. This force drives the piston downward that pushes the connecting rod which forces the crankshaft to produce the engine torque (T_e), which is also known as indicated torque. The forces acting on the piston, connecting rod, and crankshaft are shown in Fig. 6.11. Inertial forces are shown to deal with this problem as static instead of dynamic using D'Alembert's principle [6]. The piston force (F_P) is created by gas pressure in the cylinder, and it can be calculated by Eq. (6.41).

$$F_P = PA_P \tag{6.41}$$

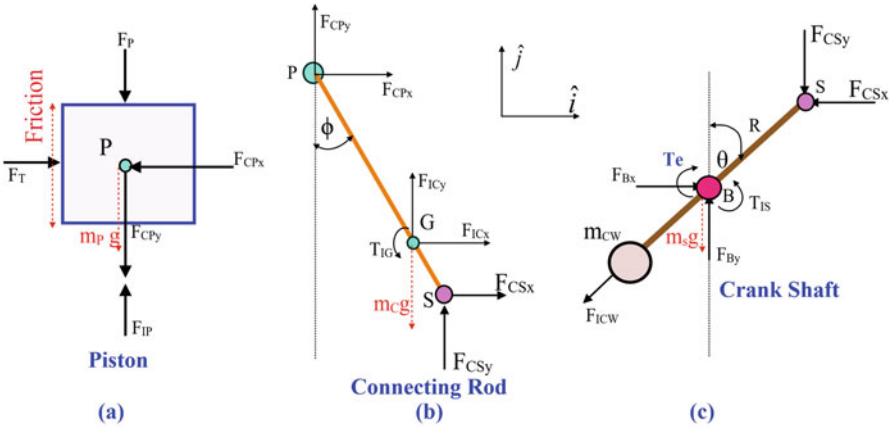

Fig. 6.11 Free body diagram of the piston, connecting rod and crankshaft of a reciprocating engine (adapted from [6])

To compute the gas torque (indicated torque), the frictional forces and gravitational forces due to the mass of components are not considered (indicated as red in Fig. 6.11). The forces acting on the piston are thrust force (F_T) from cylinder wall, inertial force due to piston acceleration (F_{IP}), and horizontal and vertical component of forces from connecting rod (F_{CPx} and F_{CPy}). The inertial force on the piston can be calculated using Eq. (6.42), where the acceleration of piston (a_P) calculated from kinematics using Eq. (6.14) and mass of piston (m_P) is known.

$$F_{IP} = m_P a_P \tag{6.42}$$

The forces on connecting rod endpoints (P and S) as well as its center of gravity (G) are shown in Fig. 6.11b. At the piston side of connecting rod, the forces are in opposite direction as of piston (F_{CPx} and F_{CPy}). The horizontal and vertical components of forces that push the crankshaft at point S are denoted as (F_{CSx} and F_{CSy}). Forces and torque on point G are inertial forces and torque that can be calculated using Eqs. (6.43) to (6.45), where mass of connecting rod (m_C) and moment of inertia about G (I_G) are known and horizontal and vertical components of acceleration (a_{Gx} and a_{Gy}) as well as angular acceleration of connecting rod (α_C) can be calculated from Eqs. (6.35) and (6.33).

$$F_{ICx} = m_C a_{Gx} \tag{6.43}$$

$$F_{ICy} = m_C a_{Gy} \tag{6.44}$$

$$T_{IG} = I_G \alpha_C \tag{6.45}$$

The forces and torque acting on crankshaft are shown in Fig. 6.11c. The forces acting on the crankshaft are the main bearing forces (F_{Bx} and F_{By}) and the forces exerted from the connecting rod at point S. The inertial torque on the crankshaft can be calculated using Eq. (6.46), where moment of inertia of crankshaft (I_s) and angular acceleration of engine/crankshaft are known.

$$T_{IS} = I_s \alpha_e \tag{6.46}$$

Engine torque can be calculated by Eq. (6.47) using torque balance around the main bearing B.

$$T_e = R\left(F_{CSy} \sin\theta - F_{CSx} \cos\theta\right) - T_{IS} \tag{6.47}$$

The Eq. (6.47) has two unknowns (F_{CSx} and F_{CSy}), which can be calculated by force and moment balance on the connecting rod (Fig. 6.11b). The force and moment balance equations are written as Eqs. (6.48)–(6.50). These three equations have four unknowns, which require an additional equation for solving. Additional Eq. (6.51) can be derived by vertical force balance on the piston (Fig. 6.11a).

$$F_{\mathrm{CSx}} + F_{\mathrm{CPx}} + F_{\mathrm{ICx}} = 0 \tag{6.48}$$

$$F_{\mathrm{CSy}} + F_{\mathrm{CPy}} + F_{\mathrm{ICy}} = 0 \tag{6.49}$$

$$F_{\mathrm{CSx}} L\cos\phi + F_{\mathrm{CSy}} L\sin\phi + T_{\mathrm{IG}} + F_{\mathrm{ICx}} l_{\mathrm{A}}\cos\phi + F_{\mathrm{ICy}} l_{\mathrm{A}}\sin\phi = 0 \tag{6.50}$$

$$F_{\mathrm{IP}} - F_{\mathrm{CPy}} - F_{\mathrm{P}} = 0 \tag{6.51}$$

Two unknowns (F_{CSx} and F_{CSy}) in the engine torque calculation equation can be computed from Eqs. (6.48) to (6.51). The engine torque can be calculated using the Eqs. (6.52) and (6.53).

$$F_{\mathrm{CSx}} = \left(F_{\mathrm{IP}} - F_{\mathrm{P}} + \frac{l_{\mathrm{B}}}{L}F_{\mathrm{ICy}}\right)\tan\phi - \frac{l_{\mathrm{A}}}{L}F_{\mathrm{ICx}} - \frac{T_{\mathrm{IG}}}{L\cos\phi} \tag{6.52}$$

$$F_{\mathrm{CSy}} = F_{\mathrm{P}} - F_{\mathrm{IP}} - F_{\mathrm{ICy}} \tag{6.53}$$

The thrust force acting on the piston by cylinder wall can also be calculated by using Eq. (6.54), which can be derived by using horizontal force balance on the piston and Eq. (6.48).

$$F_{\mathrm{T}} = -F_{\mathrm{ICx}} - F_{\mathrm{CSx}} \tag{6.54}$$

It is clear from Eq. (6.54) that the thrust force varies with crank angle position, piston mass, piston acceleration, and cylinder pressure. The thrust force acts on one side of the cylinder in the plane of connecting rod during intake and expansion stroke of the cycle. It acts on the left side (as shown in Fig. 6.11a) in clockwise rotation of the engine shaft. This is known as the major thrust side of the cylinder because of higher cylinder pressure in power stroke leading to higher thrust force. During compression and exhaust stroke, the thrust force occurs on the other side of the cylinder, which is known as the minor thrust side (anti-thrust side) [18]. Thrust force on minor thrust side is relatively lower due to lower cylinder pressure during compression and expansion strokes. The wear due to friction occurs more on the major thrust side of the cylinder wall in comparison to minor thrust side. Modern automotive engines use pistons with less mass and shorter skirts to reduce the friction.

There are simplified models of indicated torque calculations in the published literature [6, 7]. Typical indicated torque curve calculated from cylinder pressure in a single-cylinder four-stroke engine is shown in Fig. 6.12. The figure shows that the torque is higher in power stroke, and other strokes torque is lower, and this nonuniform torque requires heavier flywheel. Multicylinder engines are typically used to achieve relatively more uniform torque from the engine crankshaft. The actual variation in resultant torque depends on the number of cylinders and their firing order.

The average engine torque can be determined by taking the mean value of the torque fluctuations in one complete engine combustion cycle at particular engine

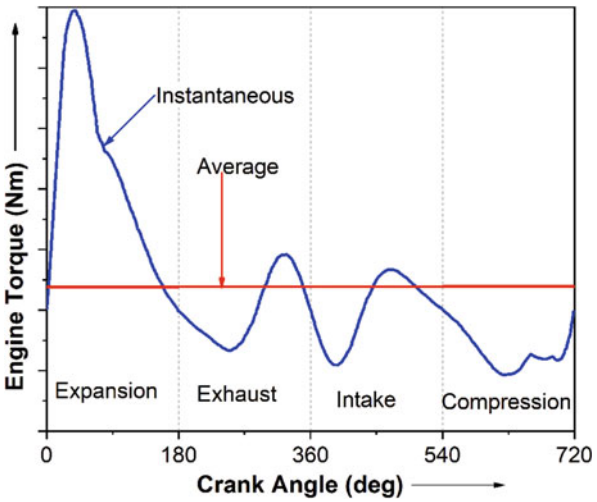

Fig. 6.12 Variation of indicated torque in a single-cylinder four-stroke engine (adapted from [6])

speed considering quasi-steady conditions. Typically, average brake torque on crankshaft is measured by engine dynamometer on a test cell. The torque and power characteristics of reciprocating engines are discussed in Sect. 6.7.

6.4 Work and Mean Effective Pressure Calculation and Analysis

In reciprocating combustion engines, work is produced by gases in the combustion chamber by moving the piston. Work is the result of a force acting through a distance, and it is typically calculated by Eq. (6.55).

$$W = \int F dx = \int P A_p dx = \int P dV \tag{6.55}$$

where P is the cylinder pressure and A_p is the piston area, and V is the volume of cylinder.

Work done in a complete engine combustion cycle can be calculated by using measured cylinder pressure data and calculated cylinder volume (Eq. 6.2) by engine geometry. Net work done in a particular engine cycle is calculated by Eq. (6.56) using measured cylinder pressure data as a function of crank angle position [19].

$$W_{net} = \frac{2\pi}{360} \int_{-360}^{360} \left(P(\theta) \frac{dV}{d\theta} \right) d\theta \tag{6.56}$$

Indicated work is typically defined as the mechanical work transferred from the gases to the piston during compression and expansion stroke, and sometimes called as gross indicated work. Indicated work can be calculated by Eq. (6.57). This work is equal to the area of the upper loop in a *P-V* diagram (Fig. 6.1b yellow region).

$$W_{\text{gross, ind}} = \frac{2\pi}{360}\int_{-180}^{180}\left(P(\theta)\frac{dV}{d\theta}\right)d\theta \tag{6.57}$$

Pumping work is the area of the lower loop in *P-V* diagram, which is a smaller area (Fig. 6.1b). Pumping work can be calculated during intake and exhaust stroke by Eq. (6.58).

$$W_{\text{pump}} = \frac{2\pi}{360}\left[\int_{-360}^{-180}\left(P(\theta)\frac{dV}{d\theta}\right)d\theta + \int_{180}^{360}\left(P(\theta)\frac{dV}{d\theta}\right)d\theta\right] \tag{6.58}$$

To compare the work output of engines of different sizes, mean effective pressure (MEP) is typically used. Mean effective pressure is same as the constant pressure, which acting on the piston is through the stroke would produce the same work per cycle as the work calculated by measured cylinder pressure by Eq. (6.57). The cylinder pressure is significant only during compression and expansion strokes in an engine combustion cycle. The work is done on the gases during compression stroke, while gases do work on the piston in the expansion stroke. Hence, net pressure would be the difference between these two. Therefore, the MEP is expected to be about the difference between the average pressures on the compression and power strokes [10]. By definition, the MEP is the ratio of work done per cycle and displacement volume (V_d) of the engine. The MEP has units of pressure, and it is a valuable measure of engine capacity to do work independent of the engine size. The MEP also depicts how well the available displacement volume of the engine is utilized for generating power.

Depending on the type of work used, different MEP parameters can be defined such as net mean effective pressure (NMEP), gross indicated mean effective pressure (IMEP), and pumping mean effective pressure (PMEP). Different parameters can be calculated by Eqs. (6.59)–(6.61).

$$\text{NMEP} = \frac{W_{\text{net}}}{V_d} \tag{6.59}$$

$$\text{IMEP} = \frac{W_{\text{ind}}}{V_d} \tag{6.60}$$

$$\text{PMEP} = \frac{W_{\text{pump}}}{V_d} \tag{6.61}$$

The IMEP is a very important and fundamental engine performance parameter that is used extensively in engine development work. The determination of IMEP

has two key elements, namely, (1) the measurement of digital cylinder pressure as a function of crankshaft position and (2) the numerical integration of the cylinder pressure and cylinder volume for calculation of work produced (Eq. 6.57). The errors in the accurate cylinder pressure measurement and numerical integration (calculation) result into the error in IMEP determination. The IMEP can be calculated by different discretized Eqs. (6.62)–(6.64) or using Simpson's method of integration [20]. Equations (6.62) and (6.63) are most commonly used in practice for calculation of IMEP.

$$\text{IMEP} = \frac{\Delta\theta}{V_\text{d}} \cdot \sum_{i=n_1}^{n_2} P(i) \cdot \frac{dV(i)}{d\theta} \tag{6.62}$$

$$\text{IMEP} = \frac{1}{2V_\text{d}} \cdot \sum_{i=n_1}^{n_2} [P(i) + P(i+1)] \cdot [V(i+1) - V(i)] \tag{6.63}$$

$$\text{IMEP} = \frac{1}{2V_\text{d}} \cdot \sum_{i=n_1}^{n_2} P(i) \cdot [V(i+1) - V(i)] \tag{6.64}$$

where $P(i)$ is the cylinder pressure at crank angle position "i," $V(i)$ is cylinder volume at crank angle position "i," V_d is the displacement volume of cylinder, n_1 is the intake BDC integer crank angle position, and n_2 is the exhaust BDC integer crank angle position.

Crank angle resolution of cylinder pressure measurement can create the difference in computed IMEP values depending on the equation used for calculation. Figure 6.13 illustrates the error in IMEP calculation using Eqs. (6.62), (6.63), and (6.64) as a function of crank angle resolution of measured cylinder pressure data, and IMEP calculation methods are labeled as method1, method2 and method3

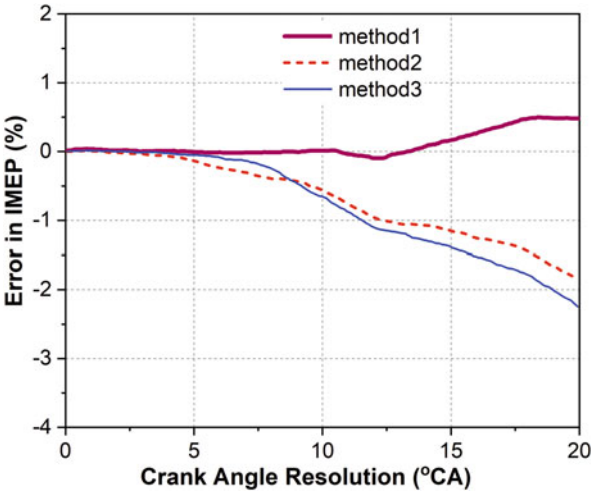

Fig. 6.13 Variation in error of IMEP calculation as a function of crank angle resolution (adapted from [20])

respectively. The figure depicts that all the equations produce similar results for crank angle resolutions up to about three degrees and significant differences are detected at higher resolutions. The differences in the accuracy are the result of the numerical integration process using different equations. Typically, encoders with crank angle resolution of one degree or less are used for the experiments, and in such case the differences in calculated IMEP are negligible (Fig. 6.13). Thus, in such cases, the equations for IMEP calculation can be selected based on computational effort and data processing time [20]. However, sometimes 60-2 teeth wheel is used for sensing the crank angle, which has the resolution of six crank angle degree, that may lead to error in IMEP calculation. The Eq. (6.62) seems to be the best IMEP calculation equation, which consistently produced the best accuracy at coarse crank angle resolutions.

Even using the best equations for IMEP calculation, the error can be introduced by random noise in pressure data or by engine operation at heavy knock conditions. The error is largest for the heavy knock and random noise cases but is always below $\pm 2\%$, even at resolutions greater than 10° [20]. This degree of error is relatively small considering the extremely large fluctuations in the pressure data, and the effects which it would have on other parameters such as pressure rise rate and mass fraction burned. The relatively small errors appeared using coarse crank angle resolution, and noisy pressure data is due to (1) lower sensitivity to cylinder pressure fluctuations around TDC because of the low rate of change of volume, and (2) the errors created for individual steps and sections of the cycle tend to cancel out over the integration period.

The contribution to the IMEP is small near to TDC and reaches a maximum typically 40° after TDC position where the maxima of the product of pressure and volume change rate occur. Figure 6.14 illustrates the percentage contribution over 10-degree steps to the final gross IMEP for a typical full-load gasoline engine. The figure depicts that the peak negative contribution occurs at about 20° before TDC,

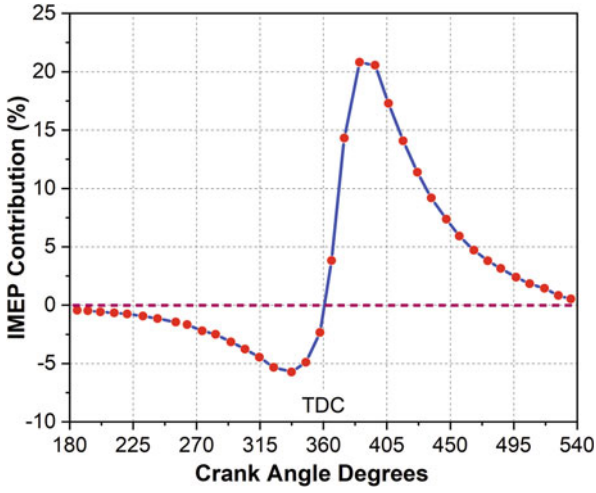

Fig. 6.14 The contribution to gross IMEP at every ten crank angle degree for full load in a typical gasoline engine (adapted from [20])

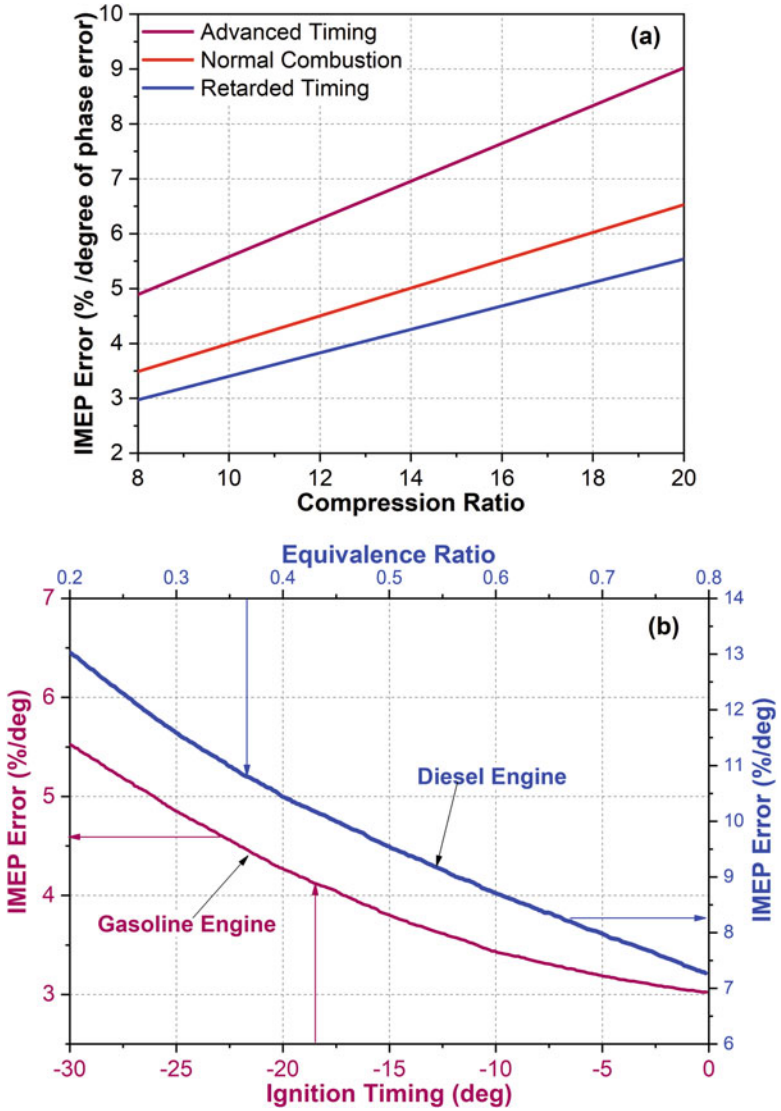

Fig. 6.15 Effect of crank angle phasing on IMEP error as a function of (**a**) compression ratio and (**b**) equivalence ratio and ignition timings (adapted from [20])

and the peak expansion stroke work occurs at about 35° after TDC position. Thus, the engine operation can be designed for maximum work output based on the contribution to IMEP on crank angle basis.

Figure 6.15 shows the effect of crank angle phasing on the error in IMEP calculations. The figure illustrates that the error of one crank angle degree in crank angle phasing can lead to a large error (up to 12%) in IMEP calculations depending on the engine operating conditions. The magnitude of the IMEP error percentage per

degree of crank angle phase shift is mainly dependent on compression ratio, heat released per unit mass of charge, ignition/injection timing, and overall combustion duration [20]. Figure 6.15a depicts that IMEP error increases linearly with compression ratio for stoichiometric engine operation of gasoline engines for different ignition timings. Figure 6.15b confirms that diesel engines will have relatively larger sensitivity than gasoline engines. Advancing the injection timing (for diesel engines) or ignition timing (for spark ignition engines) and fast-burn combustion systems increases the IMEP error for a given amount of phasing error (Fig. 6.15b). Figure 6.15b also depicts that percentage of IMEP error increases with a leaner mixture (part-load operation of a diesel engine), and thus IMEP error can easily exceed 10% error at part-load condition. A similar effect is expected with an increase in exhaust gas recirculation.

Errors in the calibration of any part of the measurement system, i.e., pressure transducer, charge amplifier, and analog-to-digital converter (ADC) will produce proportional errors in the IMEP and PMEP. Thus, calibration of the complete measurement system is required to eliminate these errors. Cylinder volume calculations as a function of crank angle position require geometrical parameters such as bore, stroke, and connecting rod length as input in the measurement system. The manufacturer does not frequently provide the connecting rod length. In case of no availability of detailed geometric data for a particular test engine, the connecting rod length is estimated, which can lead to a relatively large error in IMEP calculation. Figure 6.16 shows the error in IMEP calculation due to an error in connecting rod length (up to $\pm 10\%$). The figure shows that the IMEP error depends on the engine operating conditions, and it is a maximum of about 0.16% per 1% error in the assumed connecting rod length. For a normal range of expected errors in connecting rod length, this is a relatively small error [20].

In summary, crank angle phasing error, measurement system sensitivity, and thermal shock [21] errors are potentially the most influencing sources of error in IMEP calculation. Signal noise, connecting rod length, and crank angle resolution

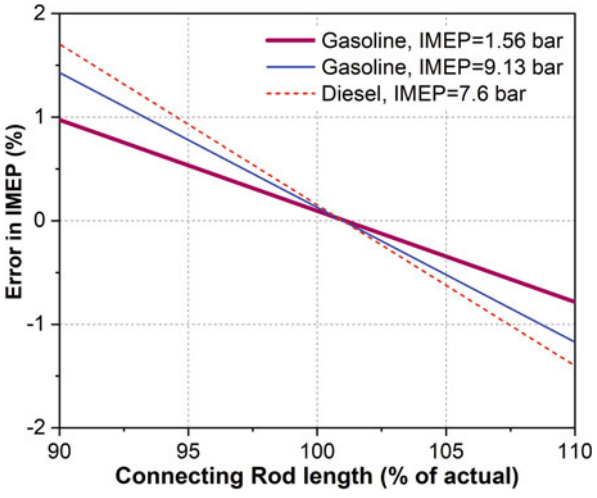

Fig. 6.16 Effect of connecting rod length on the gross IMEP calculations (adapted from [20])

errors are relatively smaller. The magnitude of IMEP errors for diesel engines is typically larger (typically twice) than the gasoline engines [20].

Determination of running quality of a reciprocating engine most significantly deals with the estimation of the IMEP, the detection of misfires and partial burns, and how the statistics of IMEP relate to customer satisfaction [22]. A poorly running engine can lead to driver discomfort because of the resulting vibrations being transmitted through the chassis and into the passenger compartment [23]. Misfires and partial burns will also dramatically affect emissions and, if left undetected, can result into catalyst damage which further worsens the situation [24]. The misfires and partial burns during engine operation also leads to drivability problems [5]. Typical methods of monitoring engine performance are based on the IMEP, and, thus, a number of ways are explored for IMEP estimation with easily measurable parameters [25–30].

To control engine torque, a conventional engine management system acquires feedback data such as air mass flow, crank position, air temperature, and air-fuel ratio. It is difficult to obtain accurate engine torque and it's precise control because these input data values are indirectly related to engine torque. Calculation of the IMEP using measured cylinder pressure data can be used to obtain more accurate torque data because IMEP is equivalent to indicated torque [28]. Thus, a real-time IMEP estimation algorithm is required for torque-based engine control.

A faster method of IMEP calculation is developed by using a very simple formula (Eq. 6.65) involving only two harmonic coefficients of the cylinder gas pressure. This equation avoids the necessity to calculate the variation of the cylinder volume, requiring less arithmetic operations than the formula based on the integration of the elemental work. The direct values of the sampled cylinder pressure are the only data required to calculate the IMEP and the harmonic coefficients of the tangential gas pressure [30].

$$\text{IMEP} = \frac{2\pi}{N}\left[\sum_{j=1}^{N} P_j \sin\theta_j + C\sum_{j=1}^{N} P_j \sin 2\theta_j\right] \tag{6.65}$$

where C is the constant determined by Eq. (6.66) using the connecting rod ratio ($\lambda = R/L$).

$$C = \frac{\lambda}{2} + \frac{\lambda^3}{8} \tag{6.66}$$

Another real-time IMEP estimation method is developed based on difference pressure integral (DPI) in the expansion stroke [28, 31]. The DPI is calculated from cylinder pressure by Eq. (6.67).

$$\text{DPI} = \sum_{k=0^\circ\ \text{aTDC}}^{180^\circ\ \text{aTDC}} \left[P_{\text{firing}}(k) - P_{\text{motoring}}(k)\right] \tag{6.67}$$

The IMEP is calculated by a linear relationship with DIP as represented by Eq. (6.68).

$$\text{IMEP} = a \cdot \text{DPI} + b \tag{6.68}$$

where constants a and b are functions of engine speed (rpm) and start of energizing (SOE) the fuel injector. The constants are obtained by regression of the measured data, and obtained functions can be represented by Eqs. (6.69) and (6.70).

$$a = a_1\text{SOE}^2 + a_2\text{SOE} + a_3\text{rpm} + a_4 \tag{6.69}$$

$$b = b_1\text{SOE} + b_2\text{rpm} + b_3 \tag{6.70}$$

At a particular engine operating condition, the work output of a reciprocating engine depends on a number of parameters, which affects the engine combustion process. Equation (6.71) presents the main parameters which affect the IMEP in a reciprocating engine [19, 32].

$$\text{IMEP} = f\left(\phi, P_{\text{in}}, \text{CA}_{50}, N, \dot{Q}_{\text{out}}, \text{fuel}, \%\text{EGR}, \text{CR}\right) \tag{6.71}$$

where ϕ is the equivalence ratio, P_{in} is the boost pressure, CA_{50} is the crank angle corresponding to 50% heat release (combustion phasing), N is the engine speed, Q_{out} is heat transfer loss rate, fuel is the used fuel type (octane/cetane), %EGR is the fraction of exhaust gas recirculation (EGR) at particular operating condition, and CR is the compression ratio of the engine.

Figure 6.17 shows the variation of IMEP with EGR at different compression ratios (CR) and intake pressures. The figure shows that engine IMEP decreases with the increase of cooled EGR rate due to the displacement of fresh air at constant throttle position. The decrease in volumetric efficiency leads to deterioration in

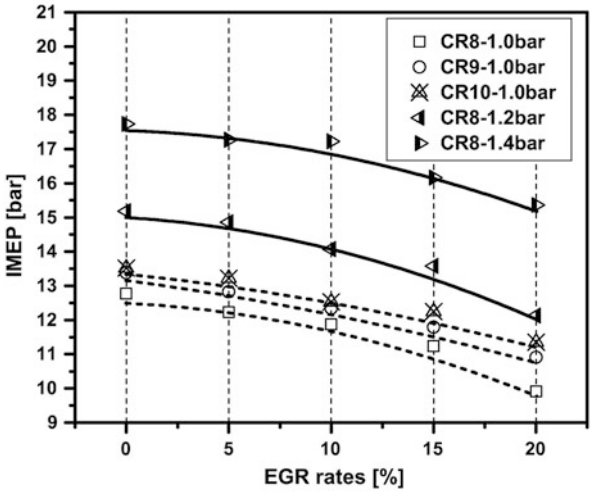

Fig. 6.17 Variation of IMEP with EGR rate for engine operation at different compression ratios and boost pressure [33]

IMEP due to stoichiometric air-fuel mixture requirement in the SI engine. Increasing the compression ratio leads to a gain in IMEP. Thus, increasing the compression ratio can recover the loss of IMEP due to EGR. The IMEP at 10% EGR rate condition is restored almost identical to that with no EGR condition by increasing the compression ratio to 10:1 (Fig. 6.17). Much more significant improvement can be found with increasing intake pressure than in compression ratio as boost pressure increases the volumetric efficiency.

Figure 6.18 shows the variation of IMEP with engine speed at full engine load in conventional gasoline and diesel engine. In a gasoline engine, full-load IMEP initially increases with engine speed, and after reaching to a peak, it starts decreasing

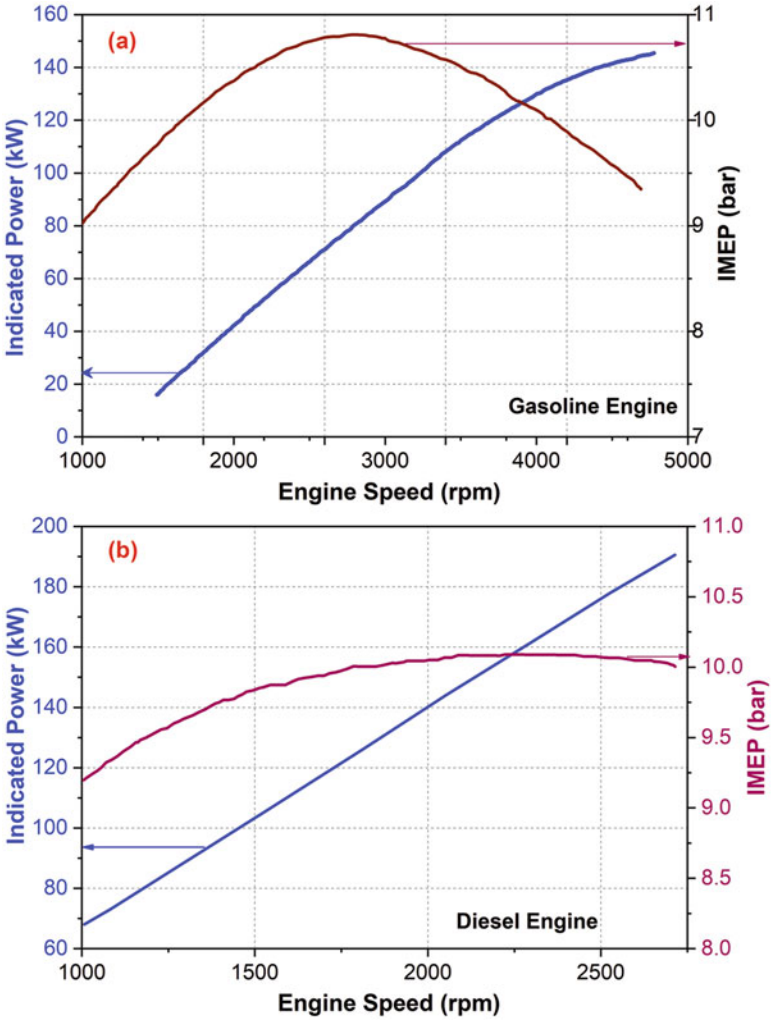

Fig. 6.18 Variation of IMEP with engine speed in a conventional (**a**) gasoline engine and (**b**) diesel engine (adapted from [5])

with engine speed (Fig. 6.18a). This trend follows the variation in volumetric efficiency, which initially increases with engine speed and decreases after a particular speed due to higher flow friction and chocking. Due to stoichiometric air-fuel operation in SI engine, the IMEP is reduced as the lower amount of fuel can be burned to produce power during engine operation at lower volumetric efficiency. In a naturally aspirated diesel engine, the IMEP vary modestly with engine speed because intake system of a diesel engine can have large flow areas. There is no throttle in a diesel engine, and the load is mainly controlled by fuel quantity. Heat transfer loss is higher at lower engine speeds. Diesel engine typically operates at overall leaner mixtures, and, thus, at higher engine speed, the same amount of fuel can be burned which results in almost constant IMEP at higher speeds (Fig. 6.18b).

The work output is mainly dependent on the amount of fuel burned, which is governed by the amount of air intake (volumetric efficiency). The quantity of fuel burned in the combustion chamber controls the pressure generated and work out of the engine in the combustion chamber. The work is also governed by displacement in addition to the pressure/force (Eq. 6.55). Therefore, combustion phasing is another major factor, which governs the work produces as it controls the effective expansion ratio. Figure 6.19 shows the effect of combustion phasing (CA_{50}) on IMEP in an HCCI combustion engine. The figure shows that for a particular λ (amount of fuel), the IMEP decrease with retarded combustion phasing. Combustion temperature is lower at retarded combustion phasing (due to high cylinder volume expansion), which leads to the higher amount of unburned fuel and lower combustion efficiency. Combustion phasing is typically controlled by intake air

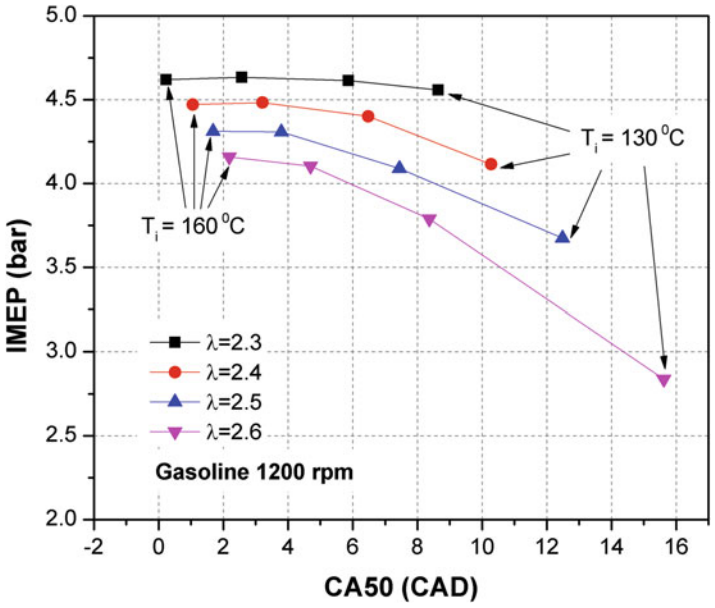

Fig. 6.19 Variation of IMEP with combustion phasing in an HCCI engine (adapted from [34, 35])

temperature in HCCI engine. Higher inlet temperature results into advanced combustion phasing, and advanced combustion phasing (close to TDC position) leads to higher IMEP (Fig. 6.19).

6.5 Engine Efficiency Analysis

Analysis of engine efficiency is an integral part of research and development work. Efficiency analysis helps to compare the improvement occurred by changes in engine design, fuel, combustion mode, and engine operating conditions. Understanding of complete energy flow through different engine components is required before performing the efficiency analysis. Figure 6.20 illustrates the energy transfer through different parts of the engine. Energy input in the engine is in the form of chemical energy stored in the fuel. Chemical energy is converted into heat energy after combustion, which is the total in-cylinder energy. A part of this energy is converted into useful work, which is the main output of the engine. Rest of the energy is utilized in the engine or comes out as heat energy, which is released in the form of heat rejected through radiator, heat rejection from the surface to ambient, and energy leaving through exhaust tail-pipe (Fig. 6.20). There are piston work transfers in and

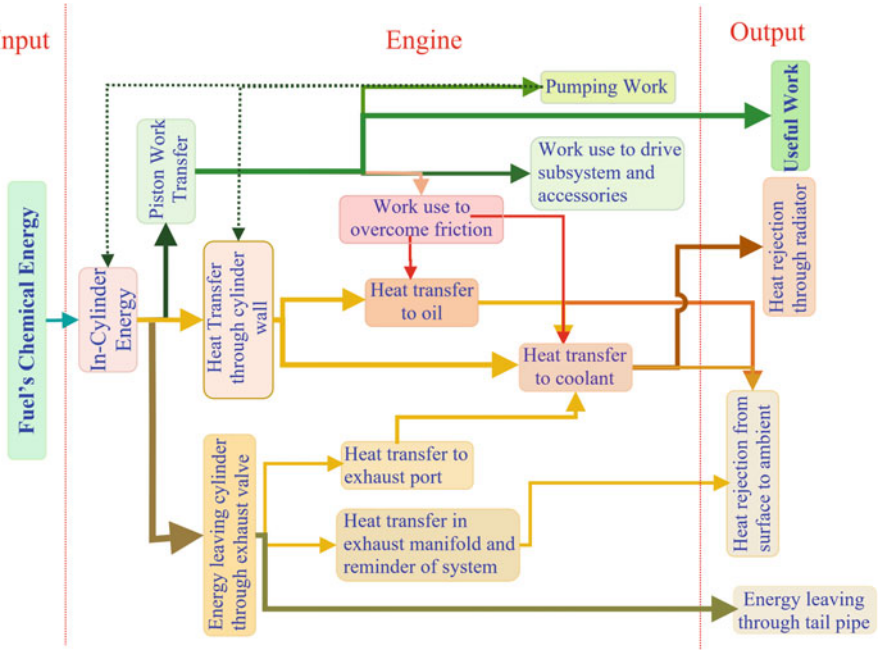

Fig. 6.20 Energy flow in through different engine components in a reciprocating internal combustion engine (adapted from [9])

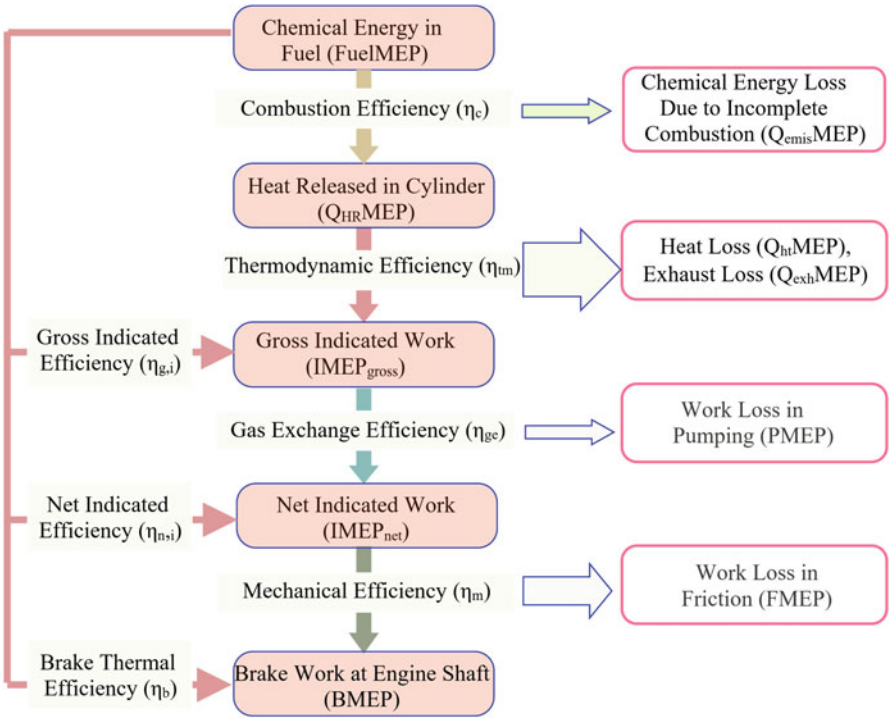

Fig. 6.21 Efficiency breakdown in a reciprocating internal combustion engine (adapted from [37, 38])

out of the engine cylinder, and net work transfer can be on the order of 40% of the fuel energy at full engine load. The net heat transfer out of the cylinder is on the order of 10–15% of the fuel energy, and the exhaust energy leaving the cylinder brings out on the order of 45–50% of the fuel energy at full-load engine operating conditions. These numbers vary significantly depending on engine operating conditions and the combustion modes [9]. Heat loss is the biggest contributor to an inefficient engine, and it occurs from several points in the engine between components. Some of the places and processes where heat loss occurs include cylinder bore to water jacket, combustion chamber deck to water jacket, piston crown to connecting rod and then to the oil, inlet valve radiated and convection, exhaust valve radiated and convection, fuel heat to fuel in evaporation, exhaust gases ejected, and blow-by losses [36].

Engine efficiency can be divided into different process efficiencies in order to find out the negatively contributing processes toward overall engine efficiency, which can be further improved. Figure 6.21 depicts the efficiency breakdown in a reciprocating internal combustion engine along with associated losses. The energy flow in the figure is presented as mean effective pressure (MEP) which is defined as the work or energy per cycle normalized by the engine's displacement volume (V_d). In a combustion engine, the chemical energy stored in the fuel is converted into heat energy during the combustion process. The energy contained by the fuel is shown as FuelMEP, which can be calculated by Eq. (6.72).

$$\text{FuelMEP} = \frac{m_f Q_{LHV}}{V_d} \tag{6.72}$$

Where m_f is the mass of fuel burned per cycle and Q_{LHV} is the lower heating value of the fuel.

The heat released (HR) during the combustion process is denoted as Q_{HR}MEP, which can be computed by integrating the heat release rate (dQ_{HR}) obtained from measured cylinder pressure (see Chap. 7).

$$Q_{HR}\text{MEP} = \frac{Q_{HR}}{V_d} = \frac{\int dQ_{HR}}{V_d} \tag{6.73}$$

The heat release during a cycle can also be estimated by measuring the unburned gas species in the exhaust and computing the chemical energy lost in unburned or partially burned species. Chemical energy lost due to incomplete combustion in the cylinder is denoted as Q_{emis}MEP. The combustion efficiency (η_c) can be defined as the ratio of heat released in the combustion chamber (Q_{HR}MEP) to total fuel energy injected (FuelMEP). The chemical energy lost is expelled out of the cylinder as partially, or completely unburnt fuel (Q_{emis}MEP) is contributing to a loss in combustion efficiency.

$$\eta_c = \frac{Q_{HR}\text{MEP}}{\text{FuelMEP}} = 1 - \frac{Q_{emis}\text{MEP}}{\text{FuelMEP}} \tag{6.74}$$

The heat released in the combustion chamber is converted to mechanical work transfer to the piston, which is denoted as gross indicated work (IMEP_{gross}). During the piston work conversion process, a fraction of the heat produced in the combustion chamber is lost in the form of heat transfer (Q_{ht}MEP) and exhaust heat through tailpipe (Q_{exh}MEP). Thermodynamic efficiency (η_{tm}) is defined as the ratio of gross indicated work to the total heat released in the cylinder as shown in Eq. (6.75). Thermodynamic efficiency is a measure of how efficiently engine can convert the heat energy of the combustion chamber into piston work.

$$\eta_{tm} = \frac{\text{IMEP}_g}{Q_{HR}\text{MEP}} = 1 - \frac{Q_{ht}\text{MEP} + Q_{exh}\text{MEP}}{\text{Q}_{HR}\text{MEP}} \tag{6.75}$$

The gross indicated efficiency ($\eta_{g,\,i}$) is defined as the ratio of gross indicated work to fuel's input energy. The relation to calculate the gross indicated efficiency is presented by Eq. (6.76).

$$\eta_{g,i} = \eta_c \cdot \eta_{tm} = \frac{\text{IMEP}_g}{\text{FuelMEP}} \tag{6.76}$$

Part of the produced indicated work is used in gas exchange process during intake and exhaust stroke. The work loss during intake and exhaust stroke is defined as pumping loss (PMEP). The gas exchange efficiency (η_{ge}) is defined as the ratio of net indicated work to the gross indicated work.

$$\eta_{ge} = \frac{IMEP_n}{IMEP_g} = 1 - \frac{PMEP}{IMEP_g} \tag{6.77}$$

The net indicated efficiency ($\eta_{n,i}$) is defined as the ratio of net indicated work to fuel's input energy. The relation to calculate the net indicated efficiency is presented by Eq. (6.78).

$$\eta_{n,i} = \eta_c \cdot \eta_{tm} \cdot \eta_{ge} = \frac{IMEP_n}{FuelMEP} \tag{6.78}$$

Different moving parts of the engine consume a fraction of the net work produced to overcome the friction, and lost work is denoted as frictional work (FMEP). The final remaining work available at the crankshaft is termed as brake work (BMEP). The measure of all the frictional processes in the engine is mechanical efficiency (η_m), which is calculated by Eq. (6.79).

$$\eta_m = \frac{BMEP}{IMEP_n} \tag{6.79}$$

The brake efficiency (η_b) is defined as the ratio of brake work available at the crankshaft to total fuel energy injected into the cylinder. The brake efficiency is calculated by Eq. (6.80), which accounts for all chemical, heat, and friction losses in the reciprocating engine.

$$\eta_b = \eta_c \cdot \eta_{tm} \cdot \eta_{ge} \cdot \eta_m = \frac{BMEP}{FuelMEP} \tag{6.80}$$

Engine efficiency depends on the various parameters such as compression ratio, combustion phasing, combustion duration, equivalence ratio of the fuel-air mixture, engine speed, engine combustion mode, etc., which governs the combustion efficiency, heat loss, and exhaust loss. Figure 6.22 shows the energy and exergy distribution in conventional diesel combustion (CDC), homogeneous charge compression ignition (HCCI), and reactivity controlled compression ignition (RCCI) engine at different combustion phasing (CA_{50}). Incomplete combustion loss is increasingly higher as combustion phasing is retarded in all the combustion modes (Fig. 6.22a). Diesel combustion shows the highest combustion efficiency (lowest incomplete combustion loss) due to heterogeneous high-temperature combustion. The HCCI and RCCI combustion have relatively lower combustion temperature and, thus, lower combustion efficiency than CDC [19]. The HCCI engine shows relatively higher combustion efficiency than RCCI engine because of total premixed fueling. The RCCI combustion is controlled by reactivity stratification by direct injection of high reactivity fuel along with premixed low reactivity fuel. Hence, the fuel-air mixture near cylinder wall is relatively leaner and less reactive in comparison to HCCI combustion conditions. The lower temperature near-wall boundary leads to higher incomplete combustion in RCCI engine than HCCI engine [39]. However,

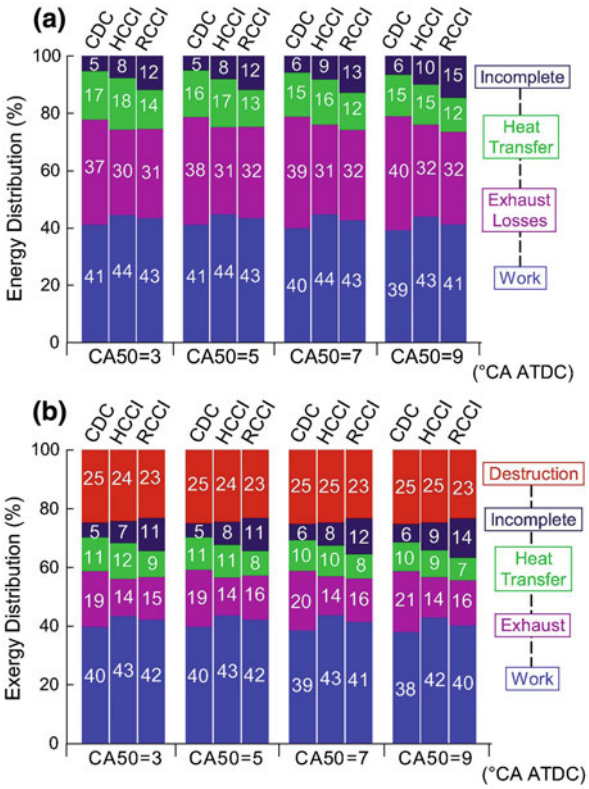

Fig. 6.22 (**a**) Energy and (**b**) exergy distributions in CDC, HCCI, and RCCI combustion mode at different combustion phasing [39]

RCCI combustion has lower heat transfer loss in comparison to CDC and HCCI combustion at constant combustion phasing (Fig. 6.22a) due to lower temperature gradient near the cylinder wall in RCCI engine. For constant combustion phasing, the exhaust losses of HCCI and RCCI are much lower than that of CDC (Fig. 6.22a), which leads to the possibility of higher work extraction. The combustion duration is lowest in HCCI combustion, which leads to highest work extraction due to close to constant volume combustion.

In comparison to results obtained from the first law of thermodynamics, second law analysis provides an extra term, i.e., exergy destruction (Fig. 6.22b). The exergy destruction is an additional restriction to the maximum achievable work from the engine. The exergy fractions of incomplete combustion, heat transfer, exhaust losses, and net work are all smaller than their corresponding energy fractions, and the overall variation trends of each part are consistent with those from the energy distribution (Fig. 6.22b).

Analysis of energy fractions of incomplete combustion, heat transfer, exhaust losses, and net work can be helpful in identifying the areas of improvement to increase the overall engine efficiency. Figure 6.23 illustrates the typical variations in thermodynamic, brake, combustion, and gas exchange efficiencies in SI and

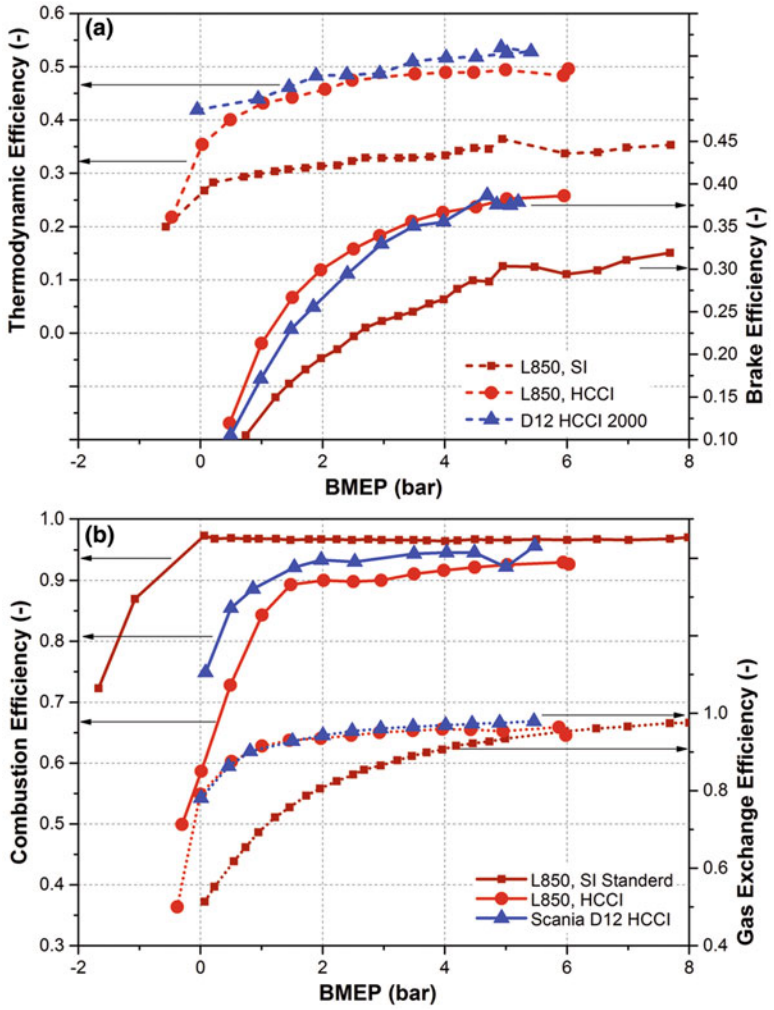

Fig. 6.23 (**a**) Thermodynamic and brake efficiency and (**b**) combustion and gas exchange efficiency as function of BMEP in HCCI engine (adapted from [40])

HCCI engine. The efficiencies can be calculated by the Eqs. (6.75), (6.80), (6.74), and (6.77), respectively. The HCCI engines show relatively higher thermodynamic efficiency as compared to SI engine due to higher compression ratio and leaner mixture operation (higher γ of working fluid). Higher thermodynamic efficiency leads to higher brake efficiency (Fig. 6.23a). Combustion efficiency increases with engine load and higher for SI engines due to high-temperature combustion (Fig. 6.23b). The gas exchange efficiency is higher in the HCCI engine due to unthrottled engine operation. The overall brake efficiency of HCCI engine is higher in comparison to SI engine. Figure 6.24 illustrates the dependency of brake

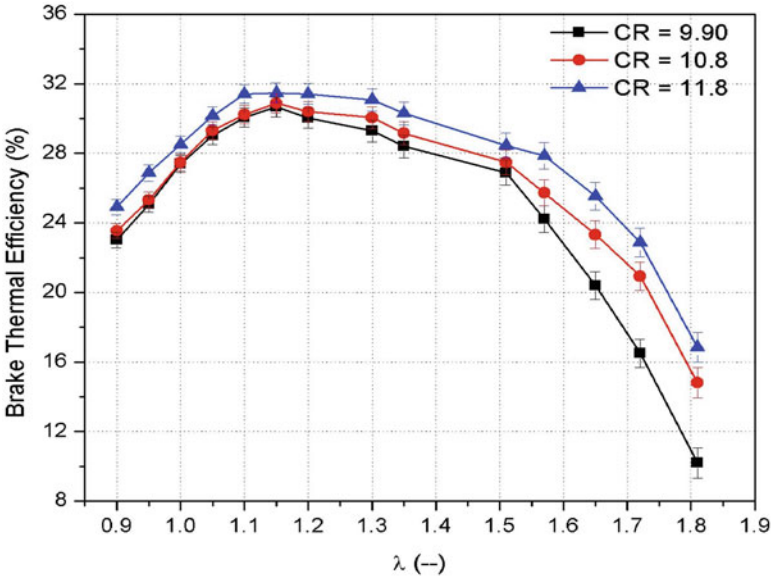

Fig. 6.24 Brake efficiency variation with relative air-fuel ratio in SI engine for different compression ratios [41]

efficiency on compression ratio and relative air-fuel ratio in SI engine. The brake efficiency is lower at richer mixture due to lower combustion efficiency. The brake efficiency reaches to a maximum and then starts decreasing with leaner mixtures (Fig. 6.24).

6.6 Gas Exchange Analysis

Cylinder pressure measurement along with intake pressure measurement can be jointly used for gas exchange analysis and the optimization of valve timings. The valve timings govern the pumping work and the residual gas fraction in the cylinder. It is well established that the gas exchange process is strongly influenced by variable valve timing (VVT), and it has the capacity to reduce the pumping loss and improve the engine performance [42, 43]. However, current VVT technologies have demerit of only changing the valve timings, i.e., valve opening (or closing) time, and cannot change the valve opening duration. Additionally, the current VVT is not able to vary the valve lift. These constraints limit the pumping loss reduction advantages using VVT technology. Another effective way to reduce the pumping loss of engine is the variable valve lift (VVL) [42]. The valve timing and valve lift both can be effectively varied as per the requirement of a particular engine operating conditions by using VVL technology. Thus, the VVL can improve the gas exchange

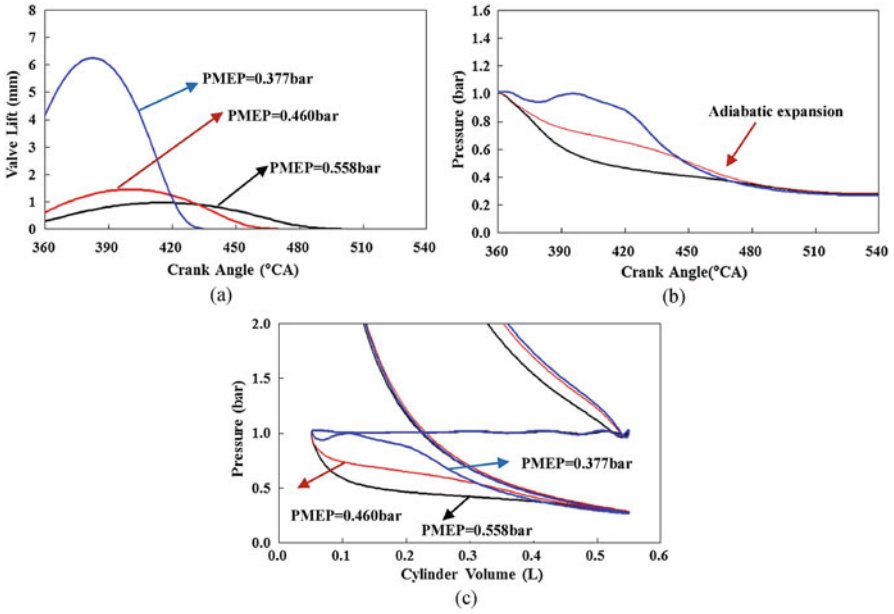

Fig. 6.25 Effects of valve lift and opening duration of the intake valve on the intake process of continuous variable valve lift engine at 2000 rpm and 2.3 bar IMEP in SI engine [42]. (**a**)Valve lift. (**b**) Cylinder pressure in intake process. (**c**) Cylinder pressure in gas exchange process

process and engine performance. The equations for computing the gas exchange efficiency and pumping work are described in Sect. 6.5.

Figure 6.25 shows the effect of intake valve lift and opening duration of continuous variable valve lift (CCVL) engine operated at 2000 rpm and 2.3 bar IMEP. The cylinder pressures at BDC position are very close to each other at all the three different valve lift conditions (Fig. 6.25) that leads to almost same engine loads. However, the intake processes for all the three lift conditions are different from each other, which leads to the difference in intake loss. Lowest valve lift and longest opening duration of the intake valve lead to large pressure loss due to the very little openness of the intake valve. This pressure drop causes the cylinder pressure much lower than intake manifold pressure which increases the pumping work (PMEP = 0.558 bar). With higher valve lift and shorter duration, the pressure loss decreases, which improves the gas exchange efficiency. At highest valve lift condition, the cylinder pressure during the intake process is approximately equal to intake manifold pressure, which leads to lowest PMEP (Fig. 6.25). Thus, cylinder pressure measurement can be used to improve and optimize the gas exchange performance of a reciprocating engine.

The variable valve lift technologies are widely used in the advanced engine combustion modes such as HCCI combustion. The VVL and VVT technologies affect the residual gas fraction in the cylinder, which affects the dilution of charge as well as the temperature of charge before combustion. In HCCI combustion,

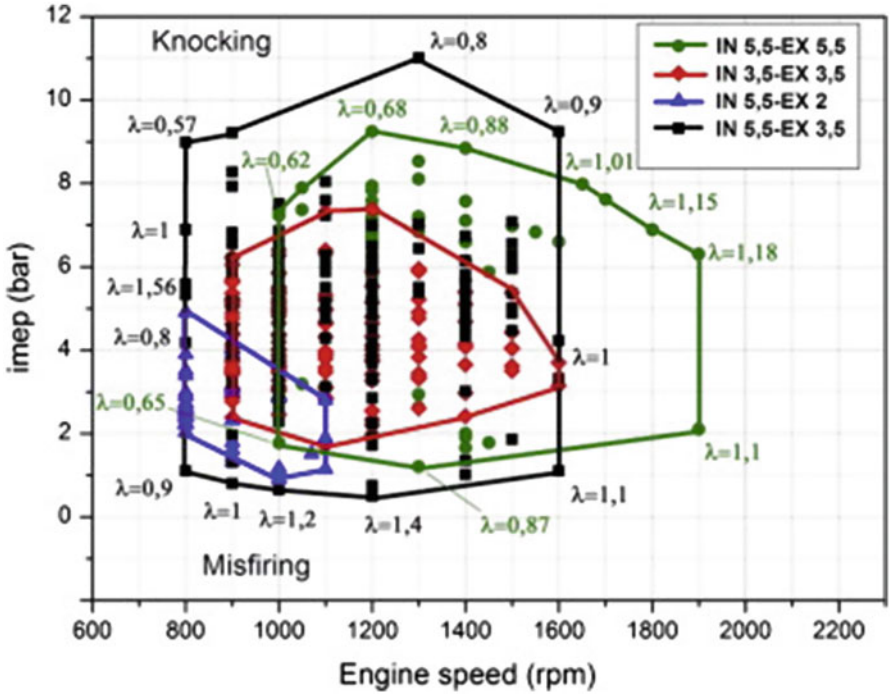

Fig. 6.26 Effects of intake and exhaust valve lifts on the HCCI operating range [44]

autoignition of leaner charge is problematic, which is improved by trapping the hot residual gases. Figure 6.26 shows the effect of intake and exhaust valve lift on the HCCI operating range. The number in the legend shows the lift in mm for intake (IN) and exhaust (EX) valves. Figure 6.26 depicts that the operating range of the HCCI engine can be extended using reduced valve lifts.

Thus, optimization of the gas exchange process helps to improve the performance of reciprocating internal combustion engines. Cylinder pressure-based combustion diagnostics of the gas exchange process is beneficial for optimizing the performance of engine.

6.7 Torque, Power and Engine Map

Torque is a good indicator of an engine's ability to do work. Torque is defined as the force acting at moment distance and has units of Nm. In other words, torque is a measure of how much a force acting on an object causes that object to rotate. Typically, torque is measured by dynamometers on an engine test cell. Different types of engine dynamometers including hydraulic, eddy current, direct current,

alternating current, and friction are used for engine testing. The engine dynamometers measure quasi-steady engine torque or average torque, not the instantaneous torque (as calculated in Sect. 6.3). The torque is measured at engine crankshaft, and, thus, it is denoted as brake torque.

Power is defined as the work per unit time, which is the rate of work of an engine. There are different kinds of power depending on the type of work is used for calculation. Typically, indicated (P_i) and brake power (P_b) are used for engine performance analysis.

$$P_i = \frac{W_i}{\text{time/cycle}} = \frac{W_i \cdot N}{X} \tag{6.81}$$

$$P_b = \frac{W_b}{\text{time/cycle}} = \frac{W_b \cdot N}{X} \tag{6.82}$$

where W_i and W_b are the indicated and brake work per cycle, respectively, N is the engine speed in revolution per second, and X is the number of revolution per cycle. The $X = 1$ for two-stroke engine and $X = 2$ for four-stroke engine.

The power equations can be represented in terms of mean effective pressure (MEP) as Eq. (6.83).

$$P = \frac{dW}{dt} = \frac{W \cdot N}{X} = \frac{\text{MEP} \cdot V_d \cdot N}{X} = \frac{\text{MEP} \cdot n \cdot A_p \cdot S \cdot N}{X} \tag{6.83}$$

where V_d is the displacement volume of the engine, n is the number of cylinders, A_p is the area of the piston, and S is the stroke length.

Specific power equations can be derived using Eq. (6.83) in terms of mean piston speed ($\overline{V}_p$).

$$\frac{P_b}{nA_p} = \text{BMEP}\frac{\overline{V}_p}{2X} \tag{6.84}$$

$$\frac{P_b}{V_d} = \text{BMEP}\frac{\overline{V}_p}{2 \cdot S \cdot X} \tag{6.85}$$

Power produced per unit piston area, often called as specific power, is typically measure of utilization of available piston area irrespective of cylinder size. Typically, current engines have specific power around 0.38 kW/cm^2, which is at mean piston speed around 15 m/s. The BMEP of naturally aspirated gasoline and diesel engines are 11–15 bar and 10 bar, respectively, and in turbocharged conditions 15–20 bar and 15–22 bar for gasoline and diesel engines, respectively. Power per unit of displacement volume (power density) is another measure that is traditionally used, and it depends on the length of stroke [10]. The Eq. (6.85) shows that the shorter stroke will have higher power output per unit volume. Typically, the power

density of naturally aspirated gasoline and diesel engines are 50–70 kW/L and 20 kW/L, respectively, and in turbocharged conditions 70–120 kW/L and 40–65 kW/L for gasoline and diesel engines, respectively. It can be noted from Eq. (6.85) that brake power can be increased in only three ways: (1) by increasing BMEP, (2) increasing total displacement volume, and (3) increasing engine speed, which is limited by material strength.

The power equations can be expressed in terms of different engine efficiencies, which provides more insight on the power generation from reciprocating engines.

$$\begin{aligned} P &= \eta_{\mathrm{b}} \cdot \dot{m}_{\mathrm{f}} \cdot Q_{\mathrm{LHV}} = \eta_{\mathrm{c}} \cdot \eta_{\mathrm{tm}} \cdot \eta_{\mathrm{ge}} \cdot \eta_{\mathrm{m}} \cdot \dot{m}_{\mathrm{f}} \cdot Q_{\mathrm{LHV}} \\ &= \eta_{\mathrm{c}} \cdot \eta_{\mathrm{i}} \cdot \eta_{\mathrm{m}} \cdot \dot{m}_{\mathrm{f}} \cdot Q_{\mathrm{LHV}} \end{aligned} \tag{6.86}$$

where $\dot{m}_{\mathrm{f}}$ is the mass flow rate of fuel and Q_{LHV} is the lower heating value of the fuel. The indicated thermal efficiency (η_{i}) can be defined in terms of thermal energy to work conversion, which is the product of thermodynamic efficiency and the gas exchange efficiency.

$$\eta_{\mathrm{i}} = \eta_{\mathrm{tm}} \cdot \eta_{\mathrm{ge}} = \frac{\mathrm{IMEP}_n}{Q_{\mathrm{HR}}\mathrm{MEP}} \tag{6.87}$$

The power term can also be represented in terms of air flow rate by Eq. (6.88).

$$P = \eta_{\mathrm{c}} \cdot \eta_{\mathrm{i}} \cdot \eta_{\mathrm{m}} \cdot \dot{m}_{\mathrm{a}} \cdot (F/A) \cdot Q_{\mathrm{LHV}} \tag{6.88}$$

where $\dot{m}_{\mathrm{a}}$ is the mass flow rate of air and (F/A) is the fuel-air ratio of engine operation.

Air flow rate is an important factor governing the power produced from the engine. The displacement volume of the engine would be filled with air truly if air is an incompressible and inviscid medium. Thus, mass entering is somewhat less depending on engine speed because air is compressible and viscous medium [10]. The viscous (turbulent) pressure drop occurs in the cylinder manifold, which leads to lower density in the cylinder than the air density at the inlet of the manifold. The other major factor is the occurrence of shock at the valve opening at very high piston speed, which chocks the air flow. Considering these factors, a volumetric efficiency term is introduced, which is defined as the ratio of the actual air mass flow and the theoretical air mass that can be achieved if air is inviscid and incompressible fluid.

$$\eta_{\mathrm{v}} = \frac{\dot{m}_{\mathrm{a}}}{\rho_{\mathrm{i}} \cdot V_{\mathrm{d}} \cdot \left(\frac{N}{X}\right)} = \frac{\dot{m}_{\mathrm{a}}}{\rho_{\mathrm{i}} \cdot A_{\mathrm{p}} \cdot S \cdot n \cdot \left(\frac{N}{X}\right)} = \frac{m_{\mathrm{a}}}{\rho_{\mathrm{i}} \cdot V_{\mathrm{d}}} \tag{6.89}$$

The equation of power can be written in terms of volumetric efficiency as Eq. (6.90).

$$P = \eta_c \cdot \eta_i \cdot \eta_m \cdot \eta_v \cdot \rho_i \cdot V_d \cdot \left(\frac{N}{X}\right) \cdot (F/A) \cdot Q_{\mathrm{LHV}} \tag{6.90}$$

The Eq. (6.90) is the main equation that can be very useful in engine design. Each term of the equation suggests the way for improving the performance of the engine. The volumetric efficiency is influenced by valve timings, cam modifications (including valve lift), tuning of intake and exhaust manifold, and number of valves per cylinder. Intake air density can be increased by turbocharging/supercharging, without throttle engine operation, inter-cooling, and use of fuel with a higher heat of vaporization (typically in a port injection system). Indicated efficiency can be improved by increasing compression ratio and reducing heat loss (piston coating, varying engine geometry, as well as number of cylinders) [10]. Mechanical efficiency can be improved by using low-tension piston rings, low friction coatings, and offset in piston pin and crankshaft.

Torque is related to the work and BMEP by Eq. (6.91).

$$2\pi \cdot T = W_b = \mathrm{BMEP} \cdot \frac{V_d}{X} \tag{6.91}$$

The Eq. (6.91) illustrates that for a particular engine, there are only two ways to increase torque: (1) by increasing the BMEP and (2) increasing the total displacement volume (increase bore/stroke or number of cylinders). For in-depth analysis, the engine torque can be written in terms of engine efficiencies using Eqs. (6.90) and (6.91).

$$T = \frac{P}{2\pi \cdot N} = \left(\frac{1}{2\pi \cdot X}\right) \cdot \eta_c \cdot \eta_i \cdot \eta_m \cdot \eta_v \cdot \rho_i \cdot V_d \cdot (F/\mathrm{A}) \cdot Q_{LHV} \tag{6.92}$$

Modern automotive engines have maximum torque per displacement volume in the range of 80–140 Nm/L [18]. Typically, power and torque curve for a turbocharged diesel engine with common rail direct injection system is shown in Fig. 6.27.

The torque curve of an engine is mainly dependent on volumetric efficiency, heat loss, and frictional loss. At higher engine speed, typically heat transfer decreases and frictional loss increases. Diesel engine operates without throttle with larger flow areas, and, thus, volumetric efficiency has a moderate effect on the torque curve. At higher engine speed, the torque decreases mainly because of increase in frictional loss.

Figure 6.27 also shows important points on the torque and power curves. The maximum engine power ($P_{\max}$) is also known as rated power, i.e., the highest power an engine is allowed to develop in continuous operation. The engine speed (N_P) corresponding to maximum power is typically known as rated speed. The maximum engine torque is denoted as $T_{\max,}$ and its corresponding engine speed is (N_T). Engine torque at the operating point of maximum power is denoted as $T_{P_{\max}}$, and engine

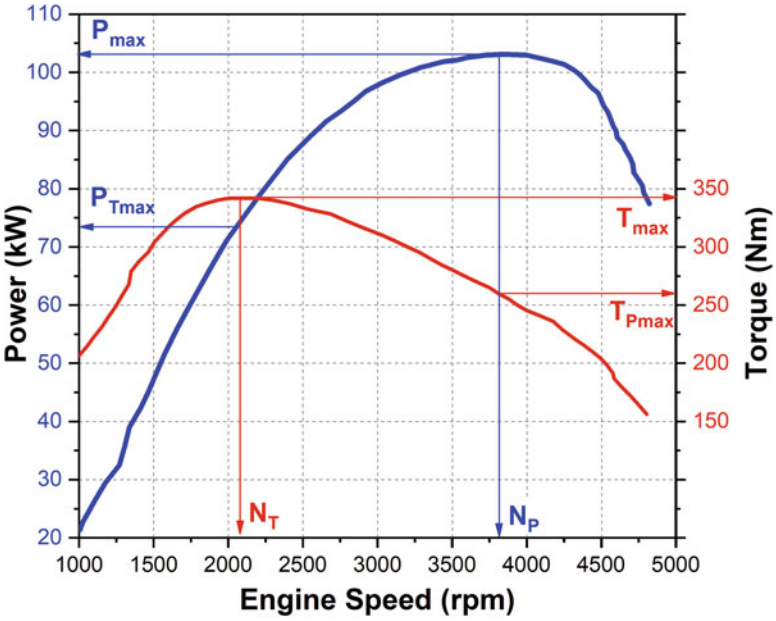

Fig. 6.27 Power curve of a modern turbocharged diesel engine (adapted from [45])

power at the operating point of maximum torque is denoted as $P_{T_{\max}}$ (Fig. 6.27). Engine torque flexibility (F_T) and engine speed flexibility (F_N) are defined by Eqs. (6.93) and (6.94) [6, 46].

$$F_T = \frac{T_{\max}}{T_{P_{\max}}} \tag{6.93}$$

$$F_N = \frac{N_P}{N_T} \tag{6.94}$$

The engine flexibility can be defined in terms of torque and speed flexibility by Eq. (6.95).

$$F_e = F_T \cdot F_N = \frac{T_{\max}}{T_{P_{\max}}} \cdot \frac{N_P}{N_T} \tag{6.95}$$

The engine with good flexibility can achieve maximum torque at lower engine speeds, or in other words, it produces higher torque at lower engine speeds. The higher engine flexibility engine will result in less frequent gear shifting [6, 46].

Figure 6.28 shows the engine torque curves for a different type of spark ignition engines. Engine torque increases as the engine is supercharged or turbocharged (Fig. 6.28a). Engine torque is proportional to the density of air (Eq. 6.92), which

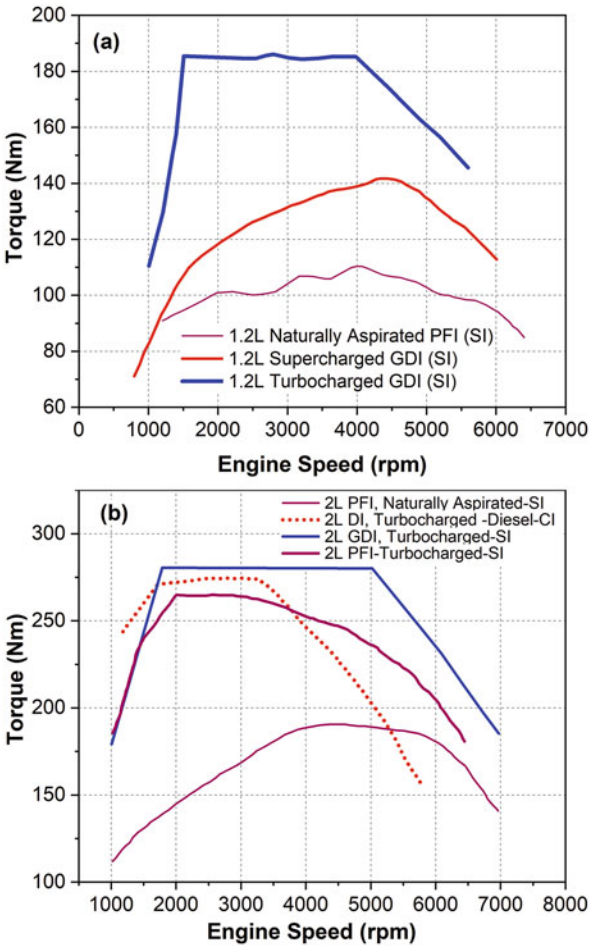

Fig. 6.28 Engine torques for various type of gasoline engines with different size (adapted from [47, 48])

increases with turbocharging that results into higher torque. Engine torque is dependent fuel injection strategy of spark ignition engine. The gasoline direct injection (GDI) engines have higher torque in comparison to the port fuel injection (PFI) engines with spark ignition (SI) as illustrated in Fig. 6.28b. It can also be observed by comparing Figure 6.28a, b that engine torque increases with an increase in displacement volume (Eq. 6.92).

The gasoline SI engine inherently operates at relatively higher engine speeds and over a wide speed range than diesel compression ignition engine (Figs. 6.27 and 6.28). Heavier components of diesel engines (due to higher peak pressures) limit their maximum engine speed. Additionally, the diesel combustion process also limits the maximum engine speed [9]. Diesel combustion occurs through a sequence of processes—atomization of liquid fuel injected into the cylinder, fuel droplets vaporization, mixing of the vaporized fuel with the surrounding air, and finally

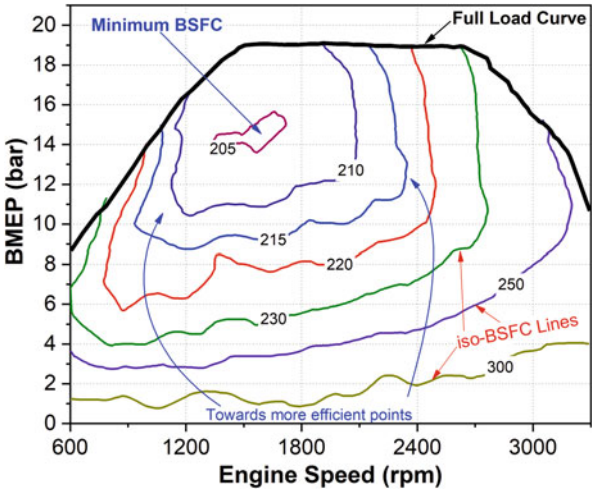

Fig. 6.29 Specific fuel consumption map of a diesel engine (adapted from [49])

autoignition of the fuel-air mixture. These processes involved in diesel combustion do not scale with engine speed. Therefore, the maximum speed of a diesel engine is also constrained by the time needed for completing the combustion during an engine cycle.

The operating point of a reciprocating internal combustion engine is characterized by its speed and its torque. The full range of all possible engine operating points in a two-dimensional presentation is known as the "engine map." In the engine map, the operating range of engine is constrained by the full-load curve and by the minimum and the maximum engine operating speed. Figure 6.29 shows a typical engine map of a diesel engine. The brake-specific fuel consumption (BSFC) is shown on the engine map. For every engine operating point on the map, a corresponding BSFC value can be determined. Several engine operating points on the speed-torque map have the same BSFC value, and locus of these points is presented as iso-BSFC lines (Fig. 6.29). Minimum specific fuel consumption typically occurs at or near full-load curve and at relatively low engine speeds. With the increase in engine speed, the engine efficiency decreases because of the rapid rate of friction increase. At lower engine speeds, the BSFC again increases due to higher heat transfer losses. Minimum BSFC typically occurs between rated and peak torque speeds.

Figure 6.30 shows the typical engine map for a gasoline engine. The trend in BSFC lines is similar to the diesel engine. The minimum specific fuel consumption is found in the lower engine speed range in the range of high engine load. The BSFC gradient increases sharply toward the low engine load range. The main reasons behind this observation are the increasing throttle losses in the SI engine and the increasing proportion of friction in relation to the useful torque output. These two factors also lead to the significant increase in BSFC at constant engine load and increasing engine speeds. Toward the full-load range, the mixture has to be enriched for two reasons: (1) to counter the knock tendency of the engine and (2) to keep the

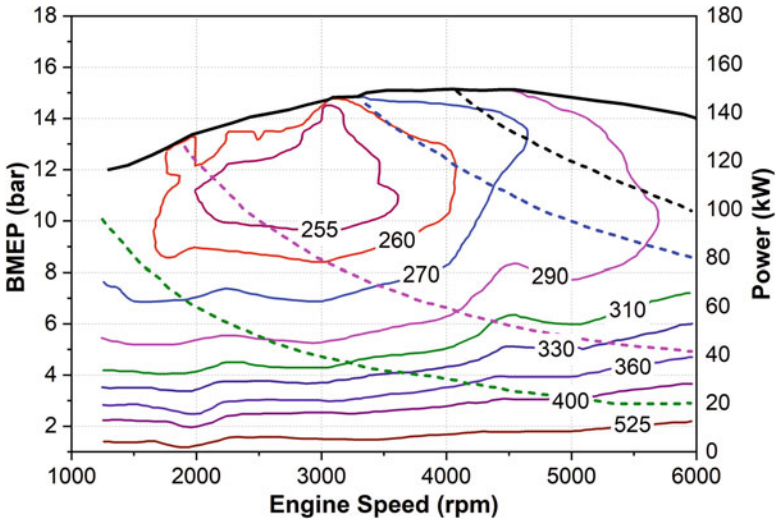

Fig. 6.30 Specific fuel consumption map of a 1.2 L gasoline SI engine (adapted from [50])

exhaust gas temperature below a critical limit temperature for catalytic converter aging. This leads to a sharper gradient of the BSFC increase in SI engine [8].

Discussion/Investigation Questions.

1. Discuss the information's revealed by the three types of presentation (P-θ, P-V, and $\log P - \log V$) of measured cylinder pressure data.
2. Discuss the sources of error in the measured pressure signal and how these sources manifested on the pressure trace. Write the possible solution for minimizing or eliminating the error from measured pressure trace.
3. Draw the P-V diagram of a naturally aspirated spark ignition engine at part-load and full-load operating conditions. Discuss how the indicating diagram will change when the engine is equipped with a turbocharger.
4. What is the difference you can observe in the P-V and P-θ diagram of conventional spark ignition and compression ignition engines?
5. Draw the cylinder pressure curve as a function of crank angle position for advanced and retarded ignition timings in a spark ignition engine. Justify the trends depicted in the graph.
6. Indicated mean effective pressure (IMEP) is typically used as indicated engine load. Write the equation for calculation of IMEP from the measured cylinder pressure sensor. Derive/define all the parameters used in the equation except measured cylinder pressure. Since pressure is measured as a digital value by the

data acquisition system, how can IMEP be calculated from digitized cylinder pressure data? Explain using digitized equations.

7. Explain why the IMEP and PMEP calculation is not affected by offset error (absolute pressure referencing) in the pressure signal measured by the piezo-electric pressure transducer.
8. Discuss and plot the differences between the ideal and actual valve timing diagram of a spark ignition engine at low and high speed. Justify the need for variable valve timings (VVT) in the engine.
9. Show by means of a diagram the energy flow in a reciprocating internal combustion engine and define combustion efficiency, indicated efficiency, mechanical efficiency, brake efficiency, and gas exchange efficiency.
10. Explain brake mean effective pressure (BMEP) and its significance. Write the typical values of BMEP for gasoline and diesel engines. Why BMEP of the naturally aspirated diesel engine is lower than a naturally aspirated spark ignition engines.
11. Suggest reasons for lower BMEP at maximum rated power as compared to BMEP at maximum torque for a given engine.
12. Why larger volume size engines (marine or locomotives) have generally higher thermal efficiency as compared to lower size engines (car or truck).
13. What are the possible ways to increase the power output of a production engine (CI and SI)?
14. Brake torque initially (at lower speed) increases with engine speed and after certain engine speed starts decreasing in engines. Suggest reasons for the given observation.
15. Engine "X" generates 45 kW of power by consuming 9 kg/h of diesel fuel. Engine "Y" generates 55 kW of power by consuming 10 kg/h which engine would one can use to do a job that required 35 kW of continuous power? Assume constant efficiency over the operating range of the both engines.
16. Mean piston speed is a parameter used for comparison of the engine of different sizes. Write the typical mean piston speed of a passenger automotive engine and a racing car engine. Discuss the major factors/parameters which are influenced by mean piston speed, which governs the engine design.
17. Typically rotation engine speed (rpm) of the diesel engine is lower in comparison to the corresponding spark ignition engines. Explain this observation and justify your answer.
18. Write the typical compression ratios for spark ignition and compression ignition engine. Discuss the typical effect of compression ratio on specific fuel consumption of an engine at particular engine operating condition.
19. Write the expression for BMEP in terms of indicated thermal efficiency, mechanical efficiency, combustion efficiency, fuel-air ratio, and intake air pressure. Discuss the ways to improve the BMEP of the engine by looking at the derived expression.
20. A designer wants to achieve 50 kW/L at 12 bar BEMP in an automotive spark ignition engine. What should stroke length be used for this particular engine? Discuss the effect of stroke length on the engine performance and design.

21. Discuss at least three thermodynamic levers that can be used for increasing the thermal efficiency of an engine.

Problems

Problem 1. A single-cylinder four-stroke engine with bore diameter "*D*," stroke "*S*," and connecting rod length "*L*" is operated at engine speed "*N*" rpm. The engine has a crank radius of "*R*" and piston pin offset "*δ*." Derive an expression for instantaneous cylinder volume, piston speed, and acceleration. Clearly state your assumptions if any.

(a) Calculate instantaneous piston speed and acceleration (without pin offset case) for $N = 1000$, 2000, and 3000 rpm for D and $S = 90$ mm and $L = 160$ mm. Plot the curves for 0–360 crank angle degree (CAD) and compare the results. Comment on the maximum piston speed position observed.
(b) Plot the ratio of instantaneous piston speed to mean piston speed for $L/R = 3$, 5, and 9 for without pin offset conditions for 0–360 CAD. Calculate the following parameter and fill the Table P6.1, and comment on your observations.
(c) Calculate instantaneous piston acceleration without pin offset for $N = 1000$, 2000, and 3000 rpm for B and $S = 90$ mm and $L = 160$ mm. Plot the curves for 0–360 crank angle degree (CAD) and compare the results.

Table P6.1 Determination of parameters related to engine geometry

Computing parameter	$L/R = 3$	$L/R = 5$	$L/R = 9$
Crank angle position of maximum piston speed			
Piston speed at 10 CAD after TDC at $N = 1500$ rpm			
Piston speed at 60 CAD after TDC at $N = 1500$ rpm			
Time duration for piston travel between 30° before and after TDC at $N = 1500$ rpm			
Time duration for piston travel between 30° after TDC to 90° after TDC at $N = 1500$ rpm			

Problem 2. A single-cylinder four-stroke engine has bore diameter 90 mm, stroke 100 mm, and connecting rod length 160 mm. Connecting rod is having CM (center of mass) 100 mm from the small end.

(a) Calculate and plot connecting rod angular speed and angular acceleration versus crank angle position of the crankshaft at engine speed 2000 and 4000 rpm.
(b) Calculate velocity and acceleration of connecting rod center of mass at engine speed 2000 rpm.

Problem 3. A four-cylinder engine produces 27 kW at engine speed of 1500 rpm. The engine generated the average torque of 120 Nm when fuel supply of one the cylinders was stopped. Assume BSFC of the engine is 340 g/kWh and the lower heating value of the fuel is 43 MJ/kg. Calculate the indicated thermal efficiency of the engine. Clearly state your assumptions in the calculation. Discuss the method of indicated thermal efficiency calculation if cutting fuel supply of one of the cylinders is not allowed or more accurate estimation of indicated thermal efficiency is required.

Problem 4. Calculate the following parameters shown in the table and fill empty values in Table P6.2. Compare and explain any significant difference between engines. Comment on the mean piston speed with respect to engine size for the given engines.

Table P6.2 Engine characteristics parameters for different size and type of engines

Engines	BMEP [bar]	Torque [nm]	Specific power output (P/A_p) [kW/m^2]	Mean piston speed [m/s]
SI; 4 S; 4 C; $D \times S = 87 \times 92$; $P_b = 65$ kW, $N = 5000$ rpm				
SI; 4 S; 6 C; $D \times S = 90 \times 80$; $P_b = 90$ kW, $N = 4800$ rpm				
SI; 4 S; 8 C; $D \times S = 85 \times 65$; $P_b = 410$ kW, $N = 8000$ rpm				
DI; 4 S; 12 C; $D \times S = 135 \times 125$; $P_b = 950$ kW, $N = 2200$ rpm				
DI; 2 S; 14 C; $D \times S = 965 \times 2490$; $P_b = 80{,}000$ kW, $N = 100$ rpm				

Problem 5. Assuming the engine specifications given below, answer the following questions.

Configuration: I6 (in-line 6 cylinder).
Displacement: 7.6 L
Peak brake power output: 156 kW @ 2400 rpm
Peak brake torque: 705 Nm @ 1450 rpm
Aspiration: Turbocharged
Combustion system: Direct injection
Compression ratio: 17:1

(a) Calculate the clearance volume (cubic centimeter, cc) for one cylinder.
(b) Assume the stroke/bore ratio is 1.2:1, what is the average piston speed at peak power output and peak torque output?
(c) If the volumetric efficiency is 1.5 due to turbo charging, what is the equivalence ratio at 2000 rpm if the fuel flow rate is 30 kg/h? Assume the stoichiometric Air-Fuel ratio is 15:1; ambient air density is 1.181 kg/m^3.

(d) Assume this engine burns diesel with a representative molecule of $C_{15}H_{32}$. Show the balanced stoichiometric chemical reaction, and calculate the stoichiometric air-fuel ratio. Assume this engine can also operate with a fuel mixture of 1/3 biodiesel ($C_{19}H_{36}O_2$), 1/3 ethanol (C_2H_5OH), and 1/3 of diesel ($C_{15}H_{32}$) by MOLE. Show the balanced stoichiometric chemical reaction and calculate the stoichiometric air-fuel ratio. Why stoichiometric air-fuel ratio decreases in the second case?.

(e) For a certain condition, the engine is operated with an air-fuel ratio of AF = 24, and the cycle can be modeled by an air-standard dual cycle. Assume 60% of the fuel burned at constant volume and 40% burned at constant pressure and the combustion efficiency is 100%. Cylinder conditions at the start of compression are $T_1 = 50\ ^\circ C$ and $P_1 = 150$ kPa. $C_v = 0.821$ kJ/kg K, $C_p = 1.108$ kJ/kg K, heating value of the fuel is $Q_{LHV} = 42{,}500$ kJ/kg. What will be the cycle thermal efficiency? If the air flow rate is 200 kg/h and the mechanical efficiency is 80%, what will be the brake power in kW for this condition? What will be the brake-specific fuel consumption (BSFC) of the engine?

(f) Assume the cycle thermal efficiency is the same as part (e) and the volumetric efficiency is 1.7 for a certain operating condition with engine speed at 1500 rpm. Each cylinder has one injector, and each injector has six nozzle holes with a diameter of 200 μm. The discharge coefficient of the injector nozzle is 0.75. Assume the fuel injection pressure is 1200 bar across the injector nozzle and the injection duration is 8 crank angle degrees. Calculate the air-fuel ratio and IMEP by assuming 98% combustion efficiency? Fuel density is 800 kg/m^3. Heating value of the fuel is $Q_{LHV} = 42{,}500$ kJ/kg**.**

(g) Assume the injection timing is 20° before TDC. Ignition delay is 0.0012 s at 1500 rpm. Assume constant volume combustion. What will be the indicated thermal efficiency if the ratio of the connecting rod to the crank radius is 4? Draw the *P-V* diagram. What if we have two injections in one cycle each with constant volume combustion? Draw a schematic *P-V* diagram and write the equation to calculate indicated thermal efficiency.

Problem 6. A four-stroke, four-cylinder, DI diesel engine having displacement volume of 2.5 L produces 200 HP at 4000 rpm in naturally aspirated conditions. The volumetric efficiency of engine is increased from 90% (naturally aspirated) to 110% (turbocharged) by boosting intake pressure twice as that for the naturally aspirated design. The air-fuel ratio is 18:1 for both turbocharged and naturally aspirated designs. What is the displacement volume required for the turbo engine to produce the same power at same rated rpm? Determine the fuel flow rate (cc/min) per cylinder per cycle for the turbocharged engine given that the density

of diesel fuel is 830 kg/m^3. For this engine at 4000 rpm, if the fuel injection started 12 CAD bTDC and lasted for 600 μs, at what crank angle did the injection end? Clearly write your assumptions, if any.

Problem 7. A fuel economy map of a reciprocating engine is shown in the Fig. P6.1. Answer the following questions based on the figure shown.

(a) Based on the engine map, identify whether this map is for a compression ignition engine or spark ignition engine and a naturally aspirated engine or a turbocharged engine. Justify your answer based on your observation in the engine map.
(b) Discuss the curve of maximum BMEP curve with increasing engine speed. Discuss the factors which affect the maximum BMEP curve.
(c) Best fuel economy point (minimum specific fuel consumption) is shown as point P. Discuss why specific fuel consumption increases with an increase in speed, increase in BMEP, and decrease in BMEP as indicated in the figure.
(d) Calculate the torque and power of the engine at minimum specific fuel consumption point assuming the displacement volume of the engine as 6.7 L.
(e) Draw the line at which the engine can operate and produce 150 kW of power. Assume continuous variable transmission is available for the engine which makes it possible to operate the engine at any speed by performing a torque conversion through variable gear ratios. Mark the best engine operating point for producing 150 kW from this engine.
(f) Assume the bore stroke ratio of 0.92 for this particular engine, and determine the best possible number of cylinder and bore diameters for this particular engine.

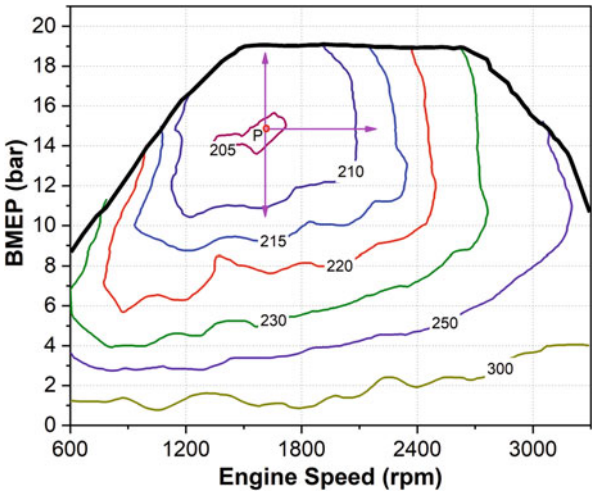

Fig. P6.1 Reciprocating engine map (adapted from [49])

Problem 8. The variation of combustion efficiency (η_c), volumetric efficiency (η_v), mechanical efficiency (η_m), thermodynamic efficiency (η_{tm}), and gross indicated efficiency ($\eta_{g,i}$) with equivalence ratio for a four-stroke, single-cylinder SI engine at wide open throttle condition is shown in Fig. P6.2. Answer the following questions based on Fig. P6.2.

(a) Justify and discuss the trend observed for variation of all the efficiencies shown in the figure.
(b) Derive the equation which relates the brake power with all the efficiency terms shown in the figure.
(c) Draw the approximate variation (trend) of brake power and brake-specific fuel consumption with equivalence ratio for this particular engine. Explain the trend drawn for both curves.

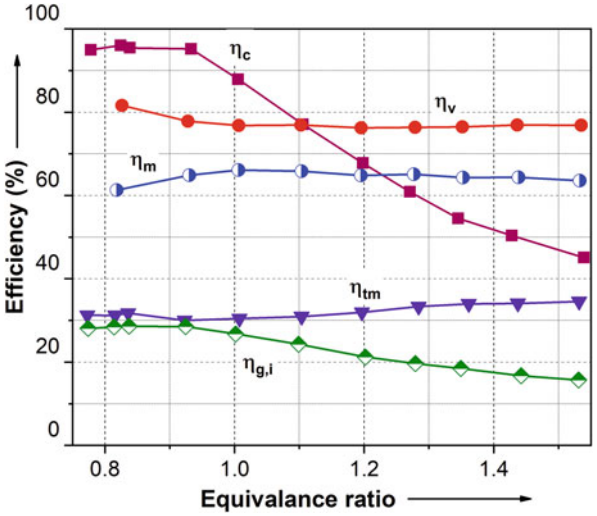

Fig. P6.2 Engine efficiency variations with equivalence ratio (adapted from [5])

Problem 9. A fuel consumption map of a four-cylinder spark ignition engine with bore/stroke of 90/80 mm is shown in Fig. P6.3. Answer the following questions based on the engine map.

(a) Fill the values of mean piston speed on the ticks shown in the figure on upper horizontal axis as shown in the figure.
(b) Draw the constant power lines on the engine map for the 10 kW, 30 kW, 50 kW, 80 kW, and 110 kW of power. Mark the most optimum point of operation for all the constant power engine operation.
(c) Draw an optimum operating line of the engine map by joining the all the fuel-efficient point on the different contours.

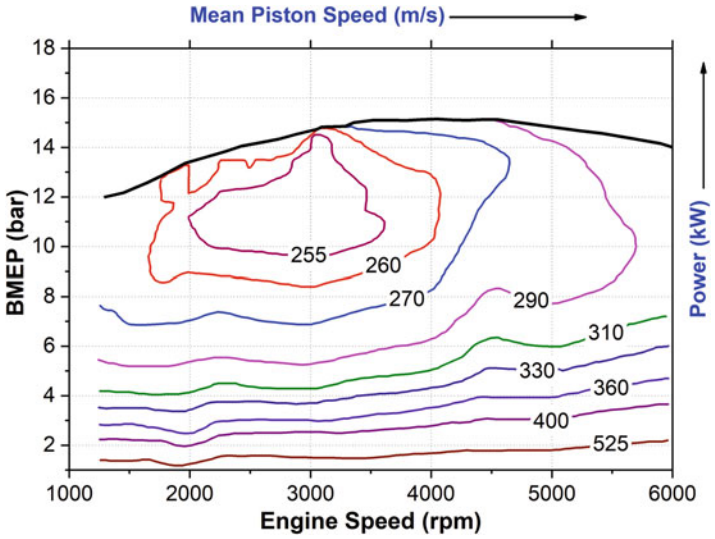

Fig. P6.3 Reciprocating engine map [50]

Problem 10. The cylinder pressure curve as a function of crank angle position for two different injection timings in an RCCI engine is shown in Fig. P6.4. Calculate the IMEP for the two conditions using Eqs. (6.62), (6.63), and (6.64) by taking 20 and 40 data points from the figure (or you can use your pressure data points for two different conditions). Write your observation and comment on the results. Discuss the role of crank angle resolution on IMEP calculation.

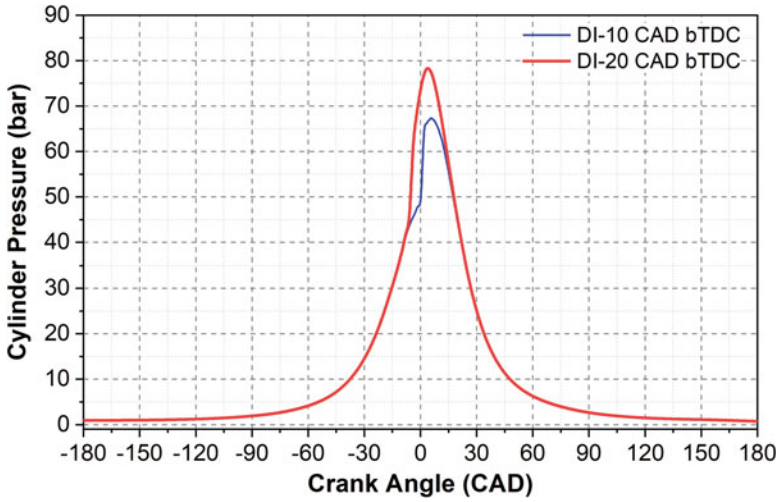

Fig. P6.4 Cylinder pressure trace at two different injection timings

Problem 11. The two engines are developed to produce the same maximum torque of 150 Nm. The torque and speed of the two engines can be assumed to be represented by equations given below. Assume the maximum engine speed of both the engines is 7000 rpm.

$$T_{e1} = 120 + 0.030(\text{rpm} - 1000) - 7.5 \times 10^{-6}(\text{rpm} - 1000)^2$$

$$T_{e2} = 120 + 0.020(\text{rpm} - 1000) - 3.33 \times 10^{-6}(\text{rpm} - 1000)^2$$

(a) Graphically plot the variation of engine torque and power with engine speed. Identify whether the engine is spark ignition or compression ignition.
(b) Calculate the engine flexibility of both the engine using Eq. (6.95). Comment in the engine flexibility of two engines.
(c) Discuss the design variations in these two engines based on the obtained torque curve.

Problem 12. Full-load torque curves for two different types of engines are given in Fig. P6.5. Assume that these engines are designed for use in the identical vehicle (same model of automotive vehicle). Identify the vehicle that provides the best acceleration from stop sign under normal conditions. Identify the vehicle which provides the maximum speed. Justify your answer with suitable reasoning. Comment on two types of engines shown in the figure.

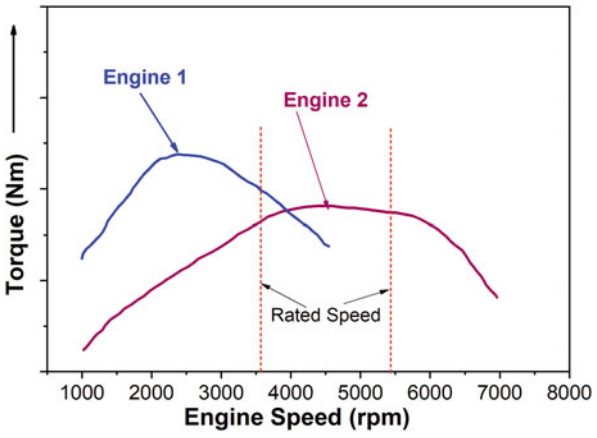

Fig. P6.5 Full-load torque curve of two different engines

Problem 13. The typical brake-specific fuel consumption curve as a function engine speed, equivalence ratio, and displacement volume are shown in Fig. P6.6. Discuss the factors influencing the variation of BSFC with each parameter, i.e., engine speed, equivalence ratio, and displacement volume. On the same graph, draw the BSFC curve at a higher compression ratio, and justify the trend with suitable reasoning.

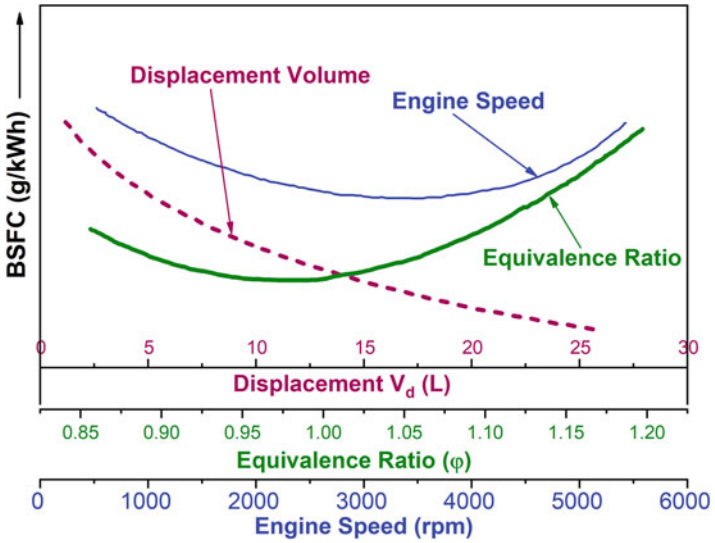

Fig. P6.6 Variation of BSFC of reciprocating engine with different engine parameters (adapted from [18])

References

1. Randolph, A. L. (1994). *Cylinder-pressure-based combustion analysis in race engines* (No. 942487). SAE Technical Paper.
2. Brunt, M. F., & Pond, C. R. (1997). *Evaluation of techniques for absolute cylinder pressure correction* (No. 970036). SAE Technical Paper.
3. Gill, P. W. S., & Ziurys, J. (1959). *Fundamentals of internal combustion engines*. New Delhi: Oxford and IBH Publishing.
4. Kar, K., Cheng, W., & Ishii, K. (2009). Effects of ethanol content on gasohol PFI engine wide-open-throttle operation. *SAE International Journal of Fuels and Lubricants, 2*(1), 895–901.
5. Heywood, J. B. (1988). *Internal combustion engine fundamentals*. New York: McGraw-Hill.
6. Crolla, D., & Mashadi, B. (2011). *Vehicle powertrain systems*. Chichester: Wiley.
7. Mallik, A. K., & Ghosh, A. (2004). *Theory of mechanism and machines*. New Delhi: Affiliated East-West Press (P) Ltd.
8. Van Basshuysen, R., & Schäfer, F. (2016). *Internal combustion engine handbook-basics, components, systems and perspectives* (2nd ed.). Warrendale: SAE International.
9. Hoag, K., & Dondlinger, B. (2016). *Vehicular engine design*. Vienna: Springer.
10. Lumley, J. L. (1999). *Engines: An introduction*. Cambridge: Cambridge University Press.
11. Park, S., & Sunwoo, M. (2003). Torque estimation of spark ignition engines via cylinder pressure measurement. *Proceedings of the Institution of Mechanical Engineers, Part D: Journal of Automobile Engineering, 217*(9), 809–817.
12. Pettersson, P. S., & Kjellin, A. (2017) *Torque estimation from in-cylinder pressure sensor for closed loop torque control* (Masters thesis). Chalmers University of Technology, Gothenburg, Sweden.
13. Rizzoni, G. (1989). Estimate of indicated torque from crankshaft speed fluctuations: A model for the dynamics of the IC engine. *IEEE Transactions on Vehicular Technology, 38*(3), 168–179.

14. Rosvall, T., & Stenlaas, O. (2016). *Torque estimation based virtual crank angle sensor* (No. 2016-01-1073). SAE Technical Paper.
15. Ginoux, S., & Champoussin, J. C. (1997). *Engine torque determination by crankangle measurements: State of the art, future prospects* (no. 970532). SAE Technical Paper.
16. Lee, B., Rizzoni, G., Guezennec, Y., Soliman, A., Cavalletti, M., & Waters, J. (2001). Engine control using torque estimation. *SAE Transactions,* Paper no - 2001-01-0995, 869–881.
17. Iida, K., Akishino, K., & Kido, K. (1990). IMEP estimation from instantaneous crankshaft torque variation. *SAE Transactions*, Paper no - 900617, 1374–1385.
18. Pulkrabek, W. W. (2004). *Engineering fundamentals of the internal combustion engine*. Upper Saddle River, NJ: Pearson Prentice Hall.
19. Maurya, R. K. (2018). *Characteristics and control of low temperature combustion engines: Employing gasoline, ethanol and methanol*. Cham: Springer.
20. Brunt, M. F., & Emtage, A. L. (1996). Evaluation of IMEP routines and analysis errors. *SAE Transactions, 960609*, 749–763.
21. Rai, H. S., Brunt, M. F., & Loader, C. P. (1999). *Quantification and reduction of IMEP errors resulting from pressure transducer thermal shock in an SI engine* (No. 1999-01-1329). SAE Technical Paper.
22. Arbuckle, J. S. (2006). *Indicated mean effective pressure estimation with applications to adaptive calibration* (PhD thesis). Michigan Technological University, Michigan, USA.
23. Hoard, J., & Rehagen, L. (1997). *Relating subjective idle quality to engine combustion* (No. 970035). SAE Technical Paper.
24. Hallgren, B. E., & Heywood, J. B. (2003). *Effects of substantial spark retard on SI engine combustion and hydrocarbon emissions* (No. 2003-01-3237). SAE Technical Paper.
25. Nishida, K., Kaneko, T., Takahashi, Y., & Aoki, K. (2011). *Estimation of indicated mean effective pressure using crankshaft angular velocity variation* (No. 2011-32-0510). SAE Technical Paper.
26. Hamedović, H., Raichle, F., Breuninger, J., Fischer, W., Fishcer, W., Dieterle, W., . . . Böhme, J. F. (2005). IMEP-estimation and in-cylinder pressure reconstruction for multicylinder SI-engine by combined processing of engine speed and one cylinder pressure. *SAE Transactions*, Paper no - 2005-01-0053, 135–142.
27. Jaine, T., Charlet, A., Higelin, P., & Chamaillard, Y. (2002). *High frequency IMEP estimation and filtering for torque based SI engine control* (No. 2002-01-1276). SAE Technical Paper.
28. Oh, S., Kim, D., Kim, J., Oh, B., Lee, K., & Sunwoo, M. (2009). *Real-time IMEP estimation for torque-based engine control using an in-cylinder pressure sensor* (No. 2009-01-0244). SAE Technical Paper.
29. Corti, E., Moro, D., & Solieri, L. (2008). *Measurement errors in real-time IMEP and ROHR evaluation* (No. 2008-01-0980). SAE Technical Paper.
30. Taraza, D. (2000). *A faster algorithm for the calculation of the IMEP* (No. 2000-01-2916). SAE Technical Paper.
31. Oh, S., Kim, J., Oh, B., Lee, K., & Sunwoo, M. (2011). Real-time IMEP estimation and control using an in-cylinder pressure sensor for a common-rail direct injection diesel engine. *Journal of Engineering for Gas Turbines and Power, 133*(6), 062801.
32. Saxena, S. (2011). *Maximizing power output in homogeneous charge compression ignition (HCCI) engines and enabling effective control of combustion timing* (PhD Thesis). University of California, Berkeley.
33. Feng, D., Wei, H., & Pan, M. (2018). Comparative study on combined effects of cooled EGR with intake boosting and variable compression ratios on combustion and emissions improvement in a SI engine. *Applied Thermal Engineering, 131*, 192–200.
34. Maurya, R. K. (2012). *Performance, emissions and combustion characterization and close loop control of HCCI engine employing gasoline like fuels* (PhD thesis). Indian Institute of Technology, Kanpur, India.

35. Maurya, R. K., & Agarwal, A. K. (2014). Experimental investigations of performance, combustion and emission characteristics of ethanol and methanol fueled HCCI engine. *Fuel Processing Technology, 126*, 30–48.
36. Atkins, R. D. (2009). *An introduction to engine testing and development*. Warrendale: SAE International.
37. Johansson, T. (2010). *Turbocharged HCCI engine, improving efficiency and operating range* (PhD thesis). Lund University, Sweden.
38. Shah, A. (2015). *Improving the efficiency of gas engines using pre-chamber ignition* (PhD thesis). Lund University, Sweden.
39. Li, Y., Jia, M., Chang, Y., Kokjohn, S. L., & Reitz, R. D. (2016). Thermodynamic energy and exergy analysis of three different engine combustion regimes. *Applied Energy, 180*, 849–858.
40. Hyvönen, J., Wilhelmsson, C., & Johansson, B. (2006). *The effect of displacement on air-diluted multi-cylinder HCCI engine performance* (No. 2006-01-0205). SAE Technical Paper.
41. Srivastava, D. K., & Agarwal, A. K. (2018). Combustion characteristics of a variable compression ratio laser-plasma ignited compressed natural gas engine. *Fuel, 214*, 322–329.
42. Li, Q., Liu, J., Fu, J., Zhou, X., & Liao, C. (2018). Comparative study on the pumping losses between continuous variable valve lift (CVVL) engine and variable valve timing (VVT) engine. *Applied Thermal Engineering, 137*, 710–720.
43. Basaran, H. U., & Ozsoysal, O. A. (2017). Effects of application of variable valve timing on the exhaust gas temperature improvement in a low-loaded diesel engine. *Applied Thermal Engineering, 122*, 758–767.
44. Cinar, C., Uyumaz, A., Solmaz, H., & Topgul, T. (2015). Effects of valve lift on the combustion and emissions of a HCCI gasoline engine. *Energy Conversion and Management, 94*, 159–168.
45. Abe, T., Nagahiro, K., Aoki, T., Minami, H., Kikuchi, M., & Hosogai, S. (2004). *Development of new 2.2-liter turbocharged diesel engine for the EURO-IV standards* (No. 2004-01-1316). SAE Technical Paper.
46. Lechner, G., & Naunheimer, H. (1999). *Automotive transmissions: Fundamentals, selection, design and application*. New York: Springer.
47. Kobayashi, A., Satou, T., Isaji, H., Takahashi, S., & Miyamoto, T. (2012). *Development of new I3 1.2 L supercharged gasoline engine* (No. 2012-01-0415). SAE Technical Paper.
48. Shinagawa, T., Kudo, M., Matsubara, W., & Kawai, T. (2015). *The new Toyota 1.2-liter ESTEC turbocharged direct injection gasoline engine* (No. 2015-01-1268). SAE Technical Paper.
49. DeRaad, S., Fulton, B., Gryglak, A., Hallgren, B., Hudson, A., Ives, D., … & Cattermole, I. (2010). *The new ford 6.7 L V-8 turbocharged diesel engine* (No. 2010-01-1101). SAE Technical Paper.
50. Fortnagel, M., Heil, B., Giese, J., Mürwald, M., Weining, H. K., & Lückert, P. (2000). Technischer Fortschritt durch Evolution—Neue Vierzylinder-Ottomotoren von Mercedes-Benz auf Basis des erfolgreichen M111 Teil 2. *MTZ-Motortechnische Zeitschrift, 61*(9), 582–590.